POLITEHNICA UNIVERSITY OF BUCHAREST

TRANSPORT DOCTORAL SCHOOL

PHD THESIS

STUDY OF WHEELSET-TRACK INTERACTION
IN RAILWAY TRACTION VEHICLES

PhD Scientific Coordinator
Prof. dr. ing. Traian MAZILU

PhD Candidate
As. ing. Marius-Alin Gheţi

DOCTORAL COMMITTEE

President:	Prof. dr. ing. Mihaela POPA
	POLITEHNICA University of Bucharest
PhD Supervisor:	Prof. dr. ing. Traian MAZILU
	POLITEHNICA University of Bucharest
Members:	1. Conf. dr. ing. Marius-Adrian SPIROIU
	POLITEHNICA University of Bucharest
	2. Prof. dr. ing. George STOICESCU
	Technical University of Civil Engineering Bucharest
	3. Prof. dr. ing. Dinel POPA
	University of Piteşti

BUCHAREST
2022

Acknowledgement: *This paper was funded by the European Social Fund from the Sectoral Operational Program Human Capital 2014-2020, through the Financial Agreement entitled "Scholarships for Entrepreneurship Education among PhD students and postdoctoral researchers (Be Entrepreneur!)", Contract no. 51680 / 09.07.2019 - SMIS Code: 124539.*

Table of contents

1. Introduction

1.1 The importance of studying interaction between the driving wheelset and track

Nowadays, rail transport is one of the most important means of transport, both for goods and for passenger transport.

Railway vehicles and the track itself are the essential components of rail transport. The two subsystems, generically called the vehicle and the railway, interact by means of contact between the wheels and the rails, and this interaction is the distinguishing element that distinguishes rail transport from any other means of transport on land.

Most of the time, the two subsystems are treated separately as stand-alone systems, and the justification for this treatment lies in the fact that the vibrations of the vehicle can be considered to be decoupled from those of the railway since the vehicle body's natural frequencies on the suspension of the vehicle are in the range of 0,5 to 20 Hz, while the frequencies of the railway are at much higher frequencies. Starting from this approach, a series of research directions have been imposed in the literature, among which it is mentioned: the vibrations of the railway vehicles, the stability of the railway vehicle running, the running quality, the vibration comfort, the dynamics of the vehicle when crossing the curves, etc., as well as those that deal with the problems of the rails: the dynamics and vibrations of the railway, the propagation through the ground of the elastic waves produced by the going trains, railway subsidence, phenomena in transition areas with variation in track stiffness, etc.m.

A number of practical aspects such as rolling noise, tread wear, shocks between wheels and rails, etc. require a different approach because the phenomena that generate them are the result of the contribution of both the vehicle's running gear and the track, and in particular the rails. These phenomena have as their source the coupled vibrations of the wheelsets and rails and therefore their treatment must start from the study of the interaction between the wheelset of the vehicle and the railway. In most situations, the vibrations of the wheelset can be considered to be disconnected from each other and even the vibrations of the wheels from the same wheelset as being also decoupled. At the same time, the vibrations of the two rails of the path are treated as independent vibrations. Under these conditions, the problem reduces to the study of the vibration of a single wheel running on a rail and for this reason, the field of research is known as *wheel-rail vibration* or *wheel-rail interaction*.

The wheel-rail vibrations develop mainly in the vertical direction being excited by the irregularities of the running surfaces and are manifesting at the level of contact between the wheel and the rail in the form of dynamic loads that are transmitted both to the track superstructure (rails, sleepers, bed) and to the running gear of the vehicle. Among the effects of wheel-rail vibrations are listed: cracking, cracks and even breaks through material fatigue to rails and wheels, cracks in sleepers, migration of broken stone components, compaction of the railway, etc.

Effects of a different nature occur when the dynamic loads produced by the wheel-rail vibrations act in the presence of slipping of the wheels on the rails. The frictional forces induced by these slips produce the wear of the track that take two forms: uniform wear and undulating wear.

In the case of driving wheelsets, the transmission of motor torque on the driveline from motor to wheelset induces torsion vibrations that are amplified especially in situations where traffic is at the adhesion limit, and torsion vibrations take the form of stick-slip vibrations. From a constructive point of view, it is preferred that the driving wheelsets are fitted with a one-sided transmission (a single geared crown mounted on the wheelset) since this type of transmission allows an increased gauge for mounting the electric traction motor compared to the bilateral transmission (two geared crowns mounted on the wheelset). The adoption of the unilateral transmission makes the driving wheelset inertial asymetrical, which facilitates the priming of torsional vibrations. Furthermore, the asymmetrical construction of the driving wheelset changes the vertical vibration regime of the wheelset on the railway in that the amplitude of the variation of the vertical contact forces is not the same on both wheels. In this way, not only is the variation of vertical contact forces a factor of excitation of a parametric nature of the torsion vibrations of the driving wheelset, but by the uneven distribution on the two wheels, it amplifies the level of these vibrations.

It should be noted that in motor vehicles, the torsional vibrations of the wheelser and its drive system, including the motor rotor, the elastic transmission shaft and the reducing gear, are coupled, by means of wheel-rail friction forces, with the rebound vibrations of the wheelset which is connected to the bogie frame by an elastic driving system to transmit the tractive force. These two types of coupled vibrations define the longitudinal vibrations of the driving wheelsets.

The torsional vibrations of the driving wheelsets affect the resistance structure of the wheelset by the variable stresses to which they are exposed. In extreme cases, uncontrolled torsional vibrations that occur at the adhesion limit in the form of stick-slip vibrations are one of the causes that produce breaks of driven wheelsets through the phenomenon of material fatigue. On the other hand, the torsional vibrations of the driving wheelset coupled with the rebound ones, as shown above, cause important variations in the traction force developed by the wheelset with negative consequences on the traction performance of the locomotives. Last but not least, the longitudinal vibrations of the driving wheelsets contribute to the priming and development of undulating wear, especially of the rails.

The direction of research on the interaction between the driving wheelset and the track represents a scientific challenge due to the multitude of aspects that need to be carefully evaluated and included in the modelling. At the same time, the interaction between the driving wheelsets and the running track is constituted as a fertile field of investigation in that the better knowledge of the main properties of the complex vibration regime of the driving wheelsets can lead to the identification of the ways and then of the means by which the negative effects of these vibrations are limited.

1.2 Scientific objectives of the thesis

The main scientific objective of the work is the study of the longitudinal vibrations of a driven wheelsets with unilateral transmission, driven by an asynchronous electric motor with the rotor in short circuit during movement at the limit of adhesion on a track in alignment and level to highlight the basic properties of the wheelset drive system in conditions where the running surfaces are affected by irregularities, and the electric traction motor works at the nominal parameters. This configuration in which the electric motor operates at the nominal parameters and the wheelset runs at the adhesion limit is very important as it is the basis for the design of the transmissions of vehicles with electric traction.

It proposes an approach that differs from other treatments by: (a) the investigation of torsional and rebound vibrations of the motor driven wheelset parametrically excited by the fluctuation of the frictional forces on the periphery of the wheels due to the variation of the normal wheel-rail contact forces, a variation caused by the vertical interaction with the track rails in the presence of surface irregularities; (b) taking into account the mechanical characteristic of the asynchronous motor in the wheelset dynamics.

The specific objectives of the thesis are:

- elaboration of the model of torsional vibrations of a driven wheelset with a unilateral transmission;
- modelling of the bending vibrations of the driving wheelset;
- modelling of the railway structure for the purpose of studying the vertical vibrations of the driving wheelset on the track;
- drawing up the model of the vertical interaction between the driving wheelset and the running track in the presence of surface irregularities;
- obtaining the vertical forces of wheel-rail contact as random functions of time;
- elaboration of the model of the longitudinal vibrations of the driving wheelset, including the drive system and its elastic driving system;
- analysis of the linear stability of the stationary regime, equivalent to the equilibrium position of the drive system of the driving wheelset and the elastic driving system;
- nonlinear analysis of the drive system of the driving wheelset and the driving system;
- analysis of longitudinal vibrations parametricly excited by variations in vertical contact forces between wheels and rails;
- experimental validation of the numerical results obtained.

1.3 The general presentation of the thesis

The paper is structured on 7 chapters, bibliography and 3 annexes covering over 270 pages, and in this section the content of each chapter are briefly presented.

1.4. Published papers

During the doctoral studies, a number of 28 papers were published: one article indexed web of science (WOS) red zone; 3 articles indexed web of science (WOS); 4 articles indexed scopus; one article indexed in other international databases; 9 articles held at national conferences.

2. State of the art on the interaction between driving wheelset and the track

In this chapter is made a review of the researches carried out in the areas of interest of the thesis subject. The main study models of wheelset vibrations are highlighted, as well as the most important models for the study of the vibrations of the railway, pointing out the advantages and limitations specific to each individual model. The most important theories and results for modeling the contact between the wheel and the rail are presented along with a series of methods for calculating the wheel-rail friction coefficient. The relevant studies addressing the interaction between the vehicle and the track are also mentioned. The chapter ends with a brief overview of the main types of electric motors used in railway traction.

3. Vibrations of the driving wheelset

For the study of the interaction between a driving wheelset and the railway track in alignment, the torsion and bending vibrations of the wheelset are important. Torsion vibrations are mainly generated by harmonic components of motor torque, while bending vibrations are mainly excited by geometric irregularities at the wheel-rail contact level. These irregularities are the leveling deviations of the track and the roughness of the running surfaces. Leveling deviations lead to low-frequency vibrations, while surface roughness is the cause of high-frequency vibrations.

Upon contact between the wheels and the rails, the torsion vibrations of the wheelset cause variations in the sliding speeds and the frictional forces. In this way, the effect of torsion vibrations has an impact on the tractive force acting in the driving system of the driving wheelset.

The bending vibrations of the driving wheelset develop mainly in the vertical plane and are accompanied by variations in the normal contact force. The size of these normal contact forces depends not only on the amplitude of geometric irregularities from the contact between the wheels and the rails, but also on the dynamic properties of the driving wheelset and the railway.

If the driving wheelset is regarded as an isolated mechanical system, the torsion vibrations are found to be decoupled from the bending vibrations. However, the real-life movement of the driving wheelset on the rails leads to the appearance of bending vibrations and variations in its normal wheel-rail contact force, due to geometric irregularities, as shown. Corroborating these aspects with the fact that the frictional force depends on the size of the normal contact force, it follows that the bending vibrations of the wheelset induce a certain regime of torsion vibrations that influence the entire drive system of the driving wheelset.

In this chapter, two models are presented, one for the study of torsion vibrations, and the other, for the study of bending vibrations of the driven wheelset. These models will be assembled together with the wheelset drive system and its steering system to form what can be called the part of the vehicle in the study model of the interaction between the driving wheelset and the railway, the other part being the railway track model.

Since they are interested in the field of low and medium frequencies, both models are based on the theory of continuous elastic body to represent the dynamics of the wheelset. Neglecting the resonant effect of the wheels and the toothed crown of the wheelset drive gear, an effect which manifests itself at high frequencies above 1500 Hz [140], the wheels and the gear's gear-toothed crown are considered to be rigid bodies attached to the wheelset body.

3.1. Mechanical model for the study of torsion vibrations

The mechanical model for the study of torsion vibrations of the driving wheelset (shown in Figure 1) consists of a free shaft of constant circular section, which has attached concentrated masses representing the two wheels and the toothed crown.

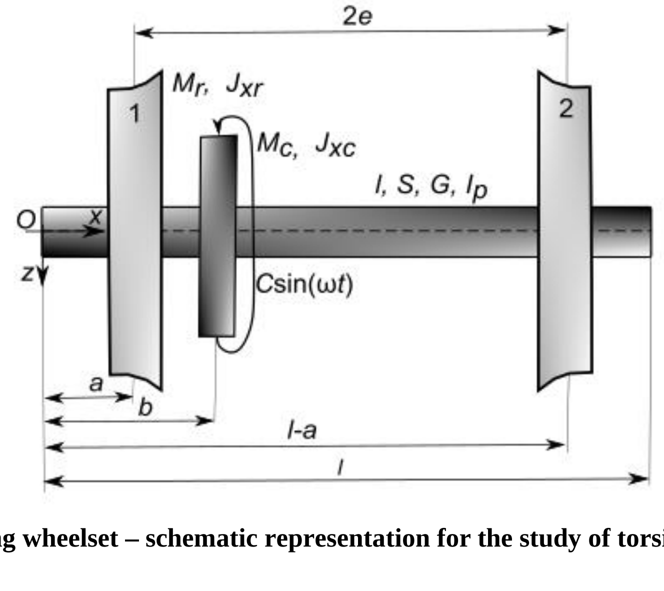

Fig. 1. Driving wheelset – schematic representation for the study of torsion vibrations.

The shaft has the length *l*, the mass per unit length equals to $m = \rho S$, where ρ is the density of the material, and *S* represents the area of the cross-section of the wheelset, and the torsion rigidity *GIp*, in which *G* is the transverse modulus of elasticity, and *the Ip* is the moment of polar inertia of the middle cross-section. The wheels have M_r mass and J_{xr} axial inertia moment, and the wheelset gear has *the* M_c mass and *the* J_{xc} axial inertia moment. The wheels are fixed at a distance *a* from the ends of the wheelset, and the gear is located at a distance *b* from the left end of the wheelset. The distance between the nominal running circles of the wheels is 2*e*. On the wheelset acts a time-varying torque, $C(t)$, applied to the toothed crown

The torsion vibration ecuation of the driving wheelset is

$$\rho I_p \frac{\partial^2\theta}{\partial t^2} - GI_p \frac{\partial^2\theta}{\partial x^2} + J_{xr} \frac{\partial^2\theta(a,t)}{\partial t^2}\delta(x-a) + J_{xr}\frac{\partial^2\theta(l-a,t)}{\partial t^2}\delta(x-l+a) + \\ + J_{xc}\frac{\partial^2\theta(b,t)}{\partial t^2}\delta(x-b) = C(t)\delta(x-b). \tag{3.1}$$

To solve this equation, the method of modal analysis is applied. The rigid vibration mode shall be taken into account together with the first two elastic modes of vibration.

3.2. Torsion frequency response of the driving wheelset

The frequency response to the driving wheelset from the LEMA electric locomotive produced by SOFTRONIC Craiova is examined.

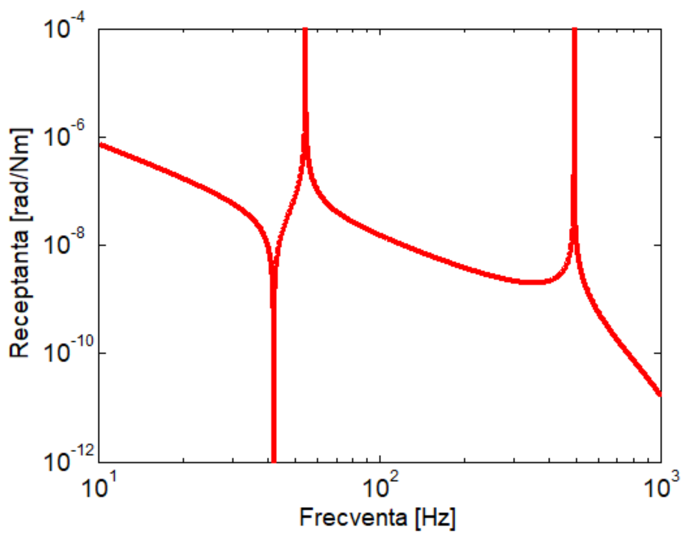

Fig. 2. Torsion receptance of the driving wheelset next to wheel 1.

With the values of the parameters of the torsion vibration model of the driving wheelset presented above, the following natural frequencies of the driving wheelset were obtained from the solution of the characteristic equation: 54.5 Hz and 494.6 Hz. From the receptance of the driving wheelset (v. fig. 2) calculated next to the first wheel, the wheel next to the geared crown, the resonance frequencies could be identified at the values corresponding to the calculated natural frequencies and an anti-resonance regime at 42,2 Hz can be identified. The existence of the anti-resonance regime is explained by the fact that the torsion waves propagate from the section where the harmonic excitation torque acts in the driven wheelset in the form of direct waves, and these waves reach the ends of the wheelset and then turn due to reflection in the form of reflected waves. The overlapping of direct and reflected waves generates stationary torsion waves. They are characterized by the existence of ventras and nodes with the specification that it is the nodes that generate the anti-resonance regime. It is noticed that at low frequency the torsion receptance is monotonously decreasing, which shows that the torsion vibration regime of the driving wheelset is dominated by the rigid mode of vibration.

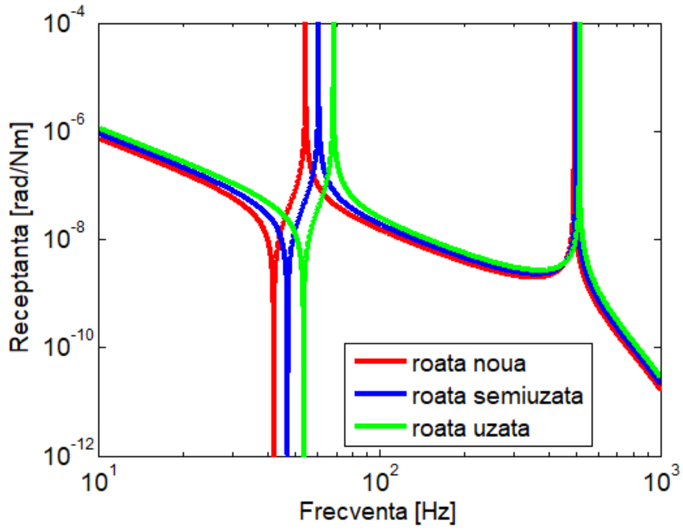

Fig. 3. Influence of the wear condition of the wheel on the torsion receptance of the driving wheelset next to wheel 1.

During the operation of the locomotive, its wheels wear out, the diameter shrinks and the mass of the wheel becomes smaller and, as a consequence, the axial inertia moment is reduced. Figure 3 shows the torsional receptance of wheel 1 for three dimeter values: 1250 mm – new wheel, 1210 mm – semi-wheel and 1170 mm – wheel at the wear limit.

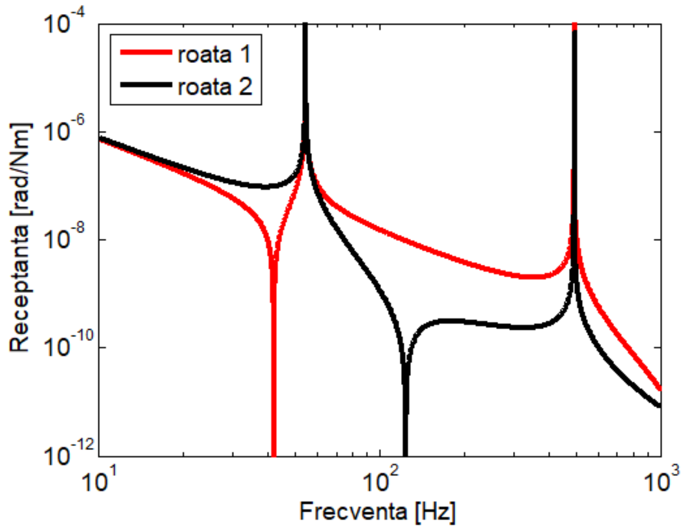

Fig. 4. Torsion reception of the driving wheelset next to the two wheels.

For the three wheel diameter values considered in the calculations, noticeable differences occur in the area of small and medium frequencies. Thus, in the case of wheels in new condition, the first resonant frequency is located at 54.5 Hz, as shown above. If the wheels are semi-worn, then the first torsion resonance frequency of the driving wheelset increases to 60.7 Hz, so that at the wheel wear limit, the first resonant frequency reaches 68.5 Hz. The receptance of the driven wheelset with worn wheels is higher in the range of rigid vibration mode. A similar tendency can also be identified in the case of the second elastic mode of vibration. The frequencies of this torsion mode are: 494.5 Hz for new wheels, 503.8 for semi-used wheels and 517.1 Hz if the wheels are at the wear limit.

Due to the asymmetry of the driving wheelset given by the fact that the position of the toothed crown is closer to one of the wheels ('wheel 1'), the torsion receptances next to the two wheels are not identical (figure 4).

Thus, it is observed that in the low frequencies domain, lower than the first resonant frequency, the torsion receptance at wheel 2 (further away from the toothed crown) is higher than the receptance of wheel 1, next to the toothed crown. However, as the frequency decreases, the two receptances become closer because the rigid torsion mode is not unbalanced – the wheels move the same way. On the other hand, in the medium and high frequencies domain, the receptance of wheel 1 is higher than the receptance of wheel 2 over almost the entire frequency range under consideration. At the same time, wheel 2 has an anti-resonance regime at a frequency higher than that observed on wheel 1 and 124 Hz respectively.

Changing the position of the toothed crown has the effect of altering the resonance frequencies of the wheelset. Thus, if the toothed crown approaches the middle of the wheelset, the frequency of the first elastic vibration mode increases from 54,6 Hz for $b = l/4$, to 55,8 Hz for $b = 3l/8$ and reaches 56,3 Hz if the position of the crown is in the middle of the wheelset. The frequency of the second elastic vibration mode decreases from 545.6 Hz to 233.9 Hz and then to 190.8 Hz. In the case of positioning the wheelset gear in the middle of it, the receptance are identical on the two wheels and have a single resonant tip, at 191 Hz. The explanation lies in the fact that the structure of the driving wheelset is asymmetrical as long as the toothed crown is not mounted in the middle of the wheelset and, due to this, the applied harmonic torque excites both symmetrical torsion modes, as well as antisymmetric ones.

3.3. Mechanical model for the study of bending vibrations

The mechanical model for the study of bending vibrations of the driving wheelset consists of a free Euler-Bernoulli beam of constant circular section, which has attached rigid bodies representing the two wheels and the wheelset gear (see Figure 5).

The beam has its mass per unit of length equal to the linear mass of the wheelset model considered for the study of torsional vibrations, $m = \rho S$, where ρ is the density of the material and S represents the cross-sectional area of the beam. Specific to the bending stress is the bending stiffness EI_y, in which E is the longitudinal elasticity modulus, and I_y is the moment of inertia of the cross-section around the bending axis. The wheels have the concentrated mass Mr

and the moment of inertia around the bending axis J_{ry}, and the gear has the concentrated mass M_c and the corresponding moment of inertia J_{cy}. Like the mechanical model for the study of torsion vibrations, the wheels are attached at a distance a from the ends of the wheelset, and the wheelset gear is located at a distance b from the left end of the wheelset. It is recalled that the distance between the nominal running circles of the wheels is $2e$.

When adopting the mechanical model of the wheelset, its variations in diameter were neglected as these variations have relatively small values. At the same time, the influence of the structural modes of vibration of the wheels, whose frequencies are much higher than the frequencies of the first two bending modes of the wheelset, has been neglected. The vertical forces $Q_1(t)$ and Q_2(t) are considered to act on the two wheels.

The motion ecuction of the driving wheelset is:

$$\begin{aligned} & EI_y \frac{\partial^4 w(x,t)}{\partial x^4} + m\frac{\partial^2 w(x,t)}{\partial t^2} + M_r\left[\frac{\partial^2 w(a,t)}{\partial t^2}\delta(x-a) + \frac{\partial^2 w(l-a,t)}{\partial t^2}\delta(x-l+a)\right] + \\ & + M_c\frac{\partial^2 w(b,t)}{\partial t^2}\delta(x-b) - J_{yr}\left[\frac{\partial^3 w(a,t)}{\partial x\partial t^2}\delta'(x-a) + \frac{\partial^3 w(l-a,t)}{\partial x\partial t^2}\delta'(x-l+a)\right] - \\ & - J_{yc}\frac{\partial^3 w(b,t)}{\partial x\partial t^2}\delta'(x-b) = Q_1(t)\delta(x-a) + Q_2(t)\delta(x-l+a). \end{aligned} \tag{3.2}$$

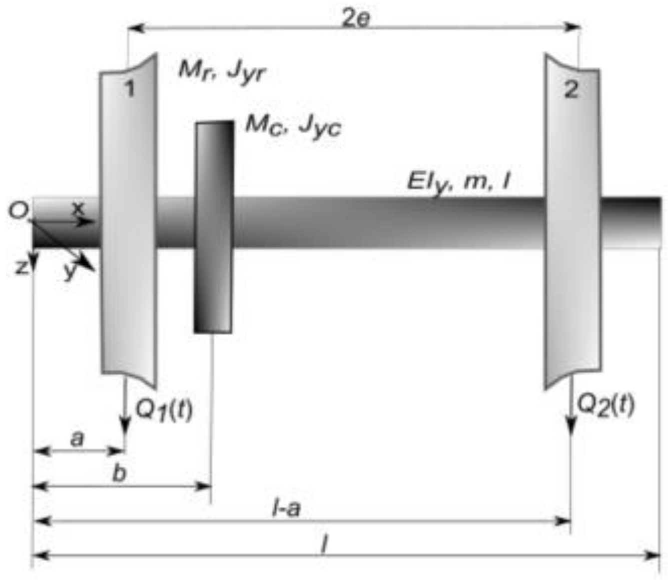

Fig. 5. Mechanical model for the study of bending vibrations.

The method of modal analysis is then applied. For the study, the first two rigid modes of vibration and the first two elastic modes of vibration are considered. The first rigid mode together with the first elastic mode of vibration are symmetrical modes, and the second rigid mode of vibration along with the second elastic mode of vibration are asymmetric modes of vibration.

3.4. Bending frequency response of the driving wheelset

In this section are analyzed the receptation diagrams obtained for the driving wheelset of the LEMA locomotive. By solving the characteristic equation, it is obtained the following natural bending frequencies of the driving wheelset: 80.3 Hz and 213.1 Hz.

In both excitation modes, the receptation diagram (Figure 6) shows the two resonant frequencies corresponding to the elastic bending modes, the first mode is symmetrical and has the resonance frequency at 80,3 Hz, and the second mode is antisymmetric with the resonance frequency at 213,1 Hz, and the receptation at wheel 2 is higher than that calculated next to wheel 1 because the centre of mass of the driving wheelset is closer to wheel 1.

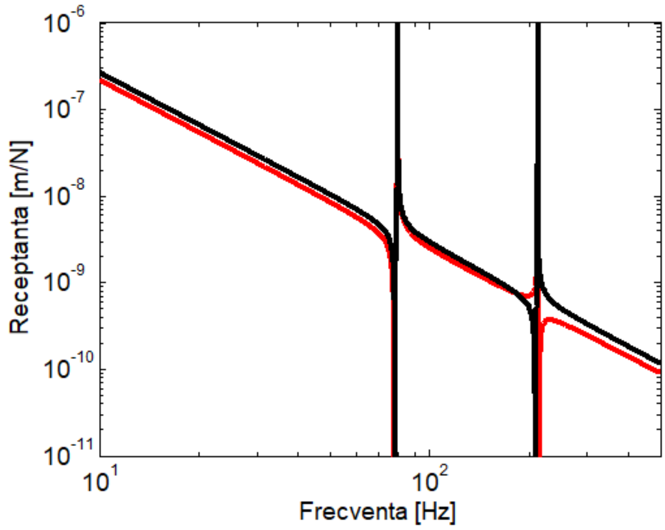

Fig. 6. Bending receptance next to the wheels – symmetrical excitation.

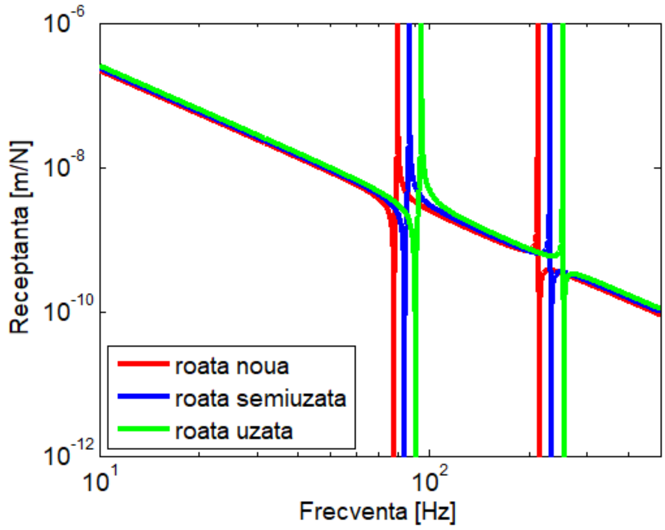

Fig. 7. The bending receptance at the right wheel for different degrees of wear – symmetrical excitation.

Unlike the torsion vibration of the driving wheelset, where the two receptance approach each other at low frequencies because the rigid torsion mode is not unbalanced, as are the elastic torsion modes, in the case of bending of the driving wheelset it is found that even at low frequencies there is a differentiation between the calculated receivers for the two wheels. The explanation lies in the fact that the bending of the wheelset has two rigid modes of vibration, the bounce and the pitch, and due to the inertial asymmetry they are excited together regardless of whether the excitation is symmetrical or antisymmetric.

As the diameter of the wheels is reduced, the bending receptances next to the wheel increases because the inertia of the driving wheelset in its assembly is less as a result of the loss of mass (see Fig. 7). Consequently, the resonant frequencies of the elastic bending modes of the driving wheelset are found at higher values. Thus, if for wheels in new condition, the resonant frequencies are at 80,3 Hz and 213,1 Hz, as stated above, these frequencies reach 87,1 Hz and 231,8 Hz respectively, if the wheels are semi-worn, and at 94,8 Hz and 253,6 Hz, when the wheels are at the wear limit.

As long as the toothed crown has an eccentric position in relation to the wheelset, both symmetrical vibration and antisymmetric vibration modes are excited regardless of the excitation mode applied to the wheels of the driving wheelset. When the toothed crown is mounted in the middle of the wheelset, the symmetric excitation mode only excites the symmetrical mode of vibration whose resonant frequency is at 76,58 Hz, and the antisymmetric excitation mode only excites the antisymmetric vibration mode that has the resonance frequency at 212,82 Hz. Consequently, the vibration regime of the driven wheelsey is lower if it has a symmetrical construction.

4. The study of vertical vibrations

In this chapter the vertical vibrations of the driving wheelset are studied when driving at constant speed on an alignment and level track in the presence of surface irregularities.

The model of vertical interaction between the driving wheelset and the running track is presented, the equations of motion in the time domain are written, and then the equations of the permanent harmonic regime are deduced and the frequency response functions are calculated.

The mechanical model of the wheelset is that presented in the previous chapter, and with its help the rigid vibration mode of the wheelset is taken into account, as well as the first two elastic modes of the bending vibration.

As for the railway model, it is based on the model of the Euler-Bernoulli beam of infinite length leaning on a continuous foundation with two elastic layers. The beam represents the rail, and the elastic layers represents the elastic and damping properties of the rail pads and the balast bed. Between the two elastic floors is inserted a layer of evenly distributed mass type, without the possibility of taking over bending and shearing efforts, to take into account the inertial effect of the sleepers.

A method of obtaining the amplitude spectrum of surface irregularities starting from the roughness level spectrum is developed.

With the help of frequency response functions and the amplitude spectrum of surface irregularities, the amplitude spectra of the interest quantities of the vertical interaction model are obtained: movement of the wheelset next to the wheels, displacement of the suspended mass above the wheels, rail displacements in the contact section and vertical contact forces.

Four scenarios are analyzed depending on the wear state of the wheels and the elasticity of the rail pads and the influence of the inertial asymmetry of the driving wheelset on the vibrational regime is highlighted.

Starting from the amplitude spectrum of vertical contact forces, their evolution in the time domain is synthesized with the help of the Fourier series, considering the initial phases of the spectral components as random functions with uniform distribution in the range [-π, π].

Vertical contact forces between the wheels and the rails, in the form of pseudo-random time components, are the excitation factor of a parametric nature at the longitudinal vibrations of the driving wheelset which are analysed in Chapter 5.

4.1. Vertical vibration model

Figure 8 shows the mechanical model for the study of the vertical vibrations of the driving wheelset which runs at a constant speed on a straight and leveled track in the presence of irregularities of the running surfaces of the rails.

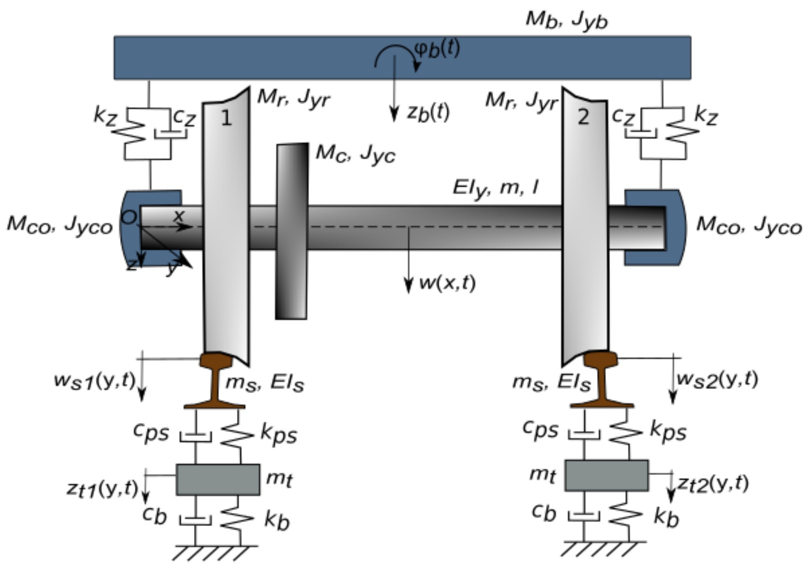

Fig. 8. The model of the vertical vibrations of the driving wheelset and the railway.

The model of the driving wheelset shown in the previous chapter is supplemented by the hanging mass of the bogie corresponding to a wheelset, the elements of the primary suspension and the wheelset boxes in order to evaluate the influence of these components of the running gear on the vertical vibrations of the driving wheelset.

The model of the railway is represented by two infinite beams of constant section, each resting on a continuous foundation with two elastic layers and a layer of distributed mass. The beams shape the two rails, and the elastic layers of the continuous foundations introduce the viscous-elastic properties of the rail pads and the ballast bed, while the distributed mass layer shapes the inertial effect of the sleepers.

The coupling of the movements of the rails by means of sleepers is neglected due to the appreciable distance between the two rails and the damping effect introduced by the ballast bed. At the same time, the influence of parametric excitation that occurs due to the fact that the sleepers are mounted at regular intervals is neglected, which leads to a change in the rigidity of the track along the distance between two sleepers. This type of excitation most influences the dynamic response of the rail in the resonant frequency range of the first way of bending the rail on the sleepers, which occurs around 1000 Hz, depending on the type of rail and the distance at which the sleepers are mounted.

According to the literature, the model used in this paper can be applied to simulate phenomena with a frequency of up to 6-700 Hz, thus covering the frequency range specific to the phenomena of interaction between the driving wheelset and the running path at the adhesion limit.

The model of the driving wheelset consists of a uniform wheelset beam, to which 5 rigid bodies corresponding to the wheels, the toothed crown and the wheelset boxes are attached. On the wheelset rests the suspended part of the bogie afferent to the wheelset that is shaped by a rigid body with two degrees of freedom, vertical translation – bounce and pitch around the longitudinal axis. The suspended mass is resting on the elements of the primary suspension which is represented by two Kelvin-Voigt-type systems; it should be noted that a Kelvin-Voigt system is made up of an elastic element that works in parallel with a viscous damping element.

The model adopted to the track shall be applied in conjunction with the model of movement of surface irregularities whereby the movement of the wheel is replaced by the movement of irregularities of the running surfaces, the wheel occupying a fixed position in relation to the track. The interaction force between the wheel and the rail has fixed support, which simplifies the calculation. This treatment is justified because the running speeds taken into account (about 70 km/h) are much lower than the propagation speed of the elastic waves through the rail and therefore do not affect practically the dynamic response of the rail.

The mathematical model of the vertical vibrations of the driving wheelset and the track must be supplemented by the equation of the contact between the wheels and the rails describing the link between the contact force, the contact deformation and the tread irregularities near the contact. Contact rigidity is calculated by linearizing hertz's nonlinear contact relationship.

Starting from the spectrum of the roughness level which, as a rule, is represented for 1/3 octave intervals of the wavelength, one can synthesize the amplitude spectrum of roughness and then be introduced into the equations of the model. As regards the phase spectrum of roughness, it can be synthesized on the basis of a series of random values contained in the range $[-\pi, \pi]$. Once the amplitude and phase spectra of roughness have been synthesized, these spectra are introduced in the form of a complex mode in the equations to obtain the spectra of the quantities of interest, namely the vertical contact forces, the displacement of the wheelset in any section of it, the displacement of the suspended mass and the displacement of the rails in the sections of contact with the wheels.

4.2. Analysis of the vertical vibrations regime

In this section is presented the analysis of the vertical vibration regime of the driving wheelset when driving on track with irregularities on the running surfaces.

The frequency response functions of the elements of interest (model without damping), the displacements of the wheels and rails in the contact sections, as well as the vertical contact forces, are different from one wheel to another due to the asymmetry of the driving wheelset (Fig. 9).

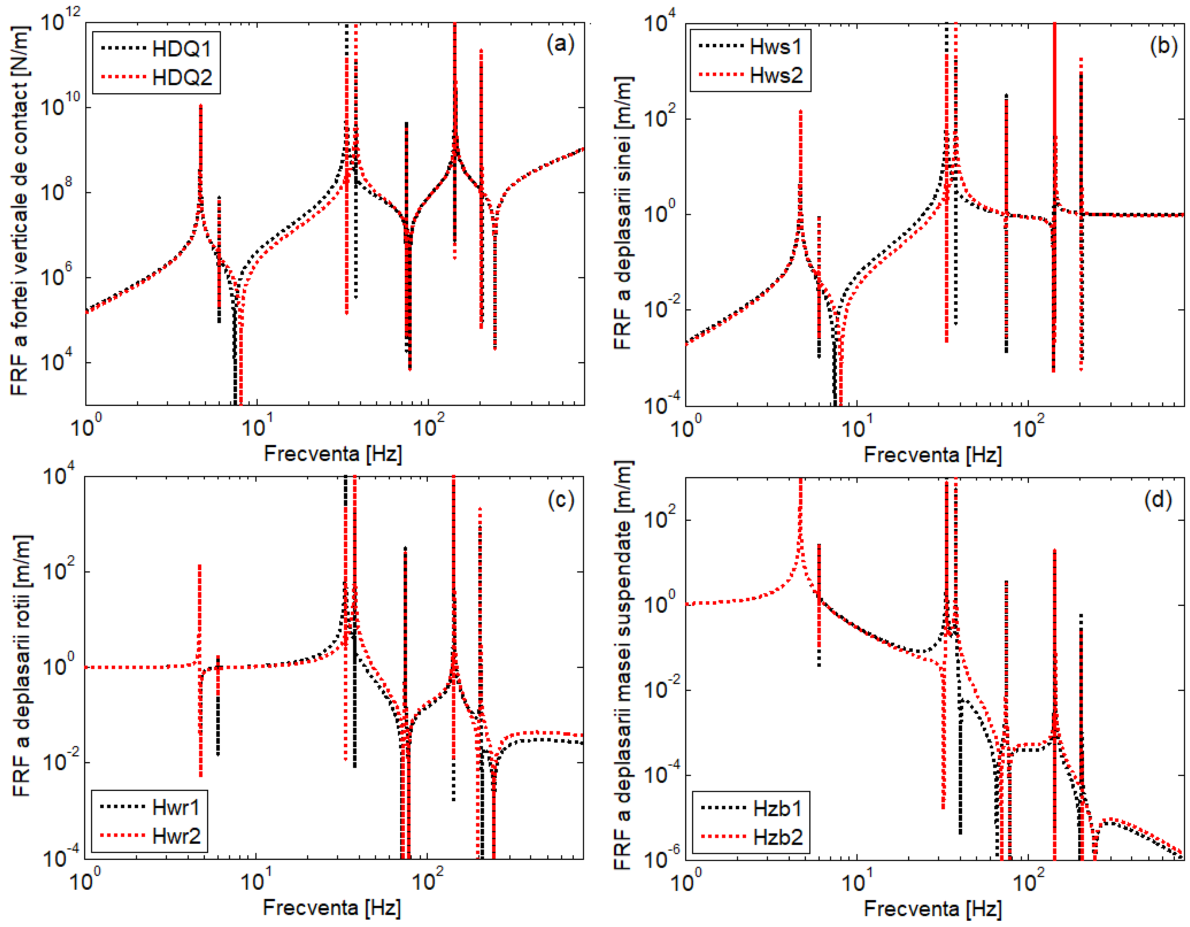

Fig. 9. Frequency response functions (without damping): (a) contact forces; (b) the movement of rails; (c) the movement of the wheelset in front of the wheels; (d) the movement of the suspended mass in front of the wheels.

Damping turns resonances into amplitude resonances, and if the resonant frequencies are close, then the peaks of the amplitude resonances are merged (e.g. bouncing and pitch of the suspended mass on the primary suspension or bouncing and the pitch of the wheelset on the track).

The effect of roughness on the vertical vibration regime of the driving wheelset and the track has been studied in correlation with the rigidity of the rail pads and the wear state of the wheels.

For the theme of this work, the most important is the vertical force of contact, and that is why only this is still referred to.

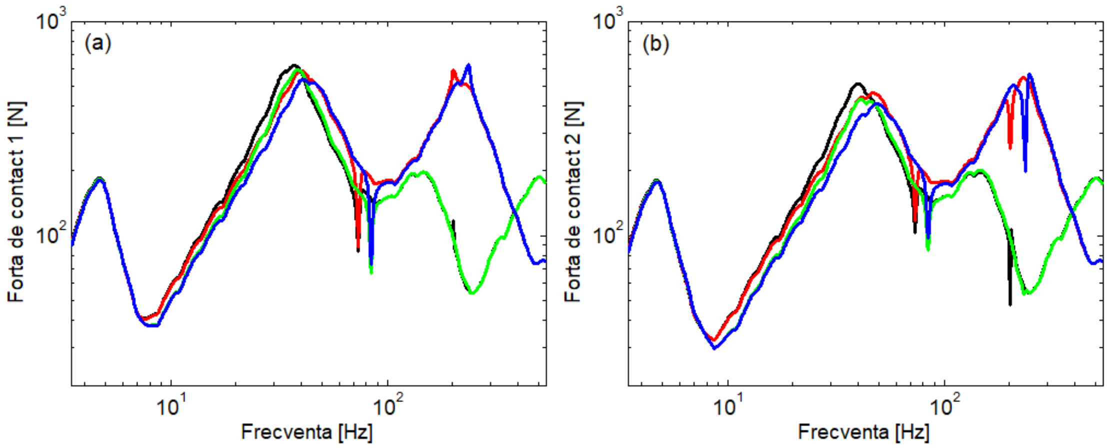

Fig. 10. Contact force spectrum: (a) at wheel 1; (b) on wheel 2; —, new wheel — elastic rail plate; - new wheel — rigid rail plate; - worn wheel - elastic rail plate; - worn wheel– rigid rail plate.

The amplitude spectrum of the vertical contact force (Figure 10) shows local highs and lows as follows. The local maximums of the vertical contact force correspond to the bouncing and pitch of the suspended mass of the bogie on the primary suspension, to the rigid modes of vibration of the wheelset on the track and to the anti-resonance regime of the rail, the frequency of the last being influenced by the rigidity of the rail plates. The local minimums of the vertical contact force are next to the resonant frequencies of the bouncing - pitch movements of the suspended mass that are coupled with those of the driving wheelset and the low and high resonance frequencies of the rail.

In the range of low frequencies, lower than the resonant frequency of the rigid modes of vibration of the wheelset on the track, the vertical contact force is greater if elastic rail plates are mounted in the track. At higher frequencies, however, the situation is reversed in the sense that the vertical contact force is lower in the case of elastic rail plates.

The wear condition of the wheels of the driving wheelset has less influence on the vertical contact forces. It may be noted, however, that at frequencies below the resonant frequency of the rigid modes of vibration of the wheelset on the track, running with new wheels is accompanied by relatively higher vertical contact forces.

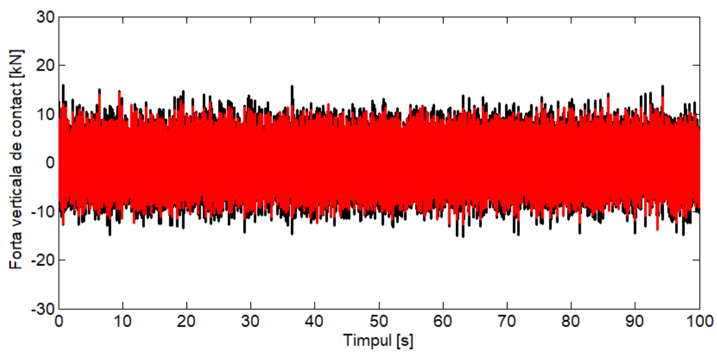

Fig. 11. Synthesis of vertical contact forces: wheel in the new state - track with elastic rail plates: —, wheel 1; —, wheel 2.

Based on the spectral components of the vertical contact forces, it is possible to synthesize their variation over time as shown in figures 11 and 12, as example. Figure 11 shows the variation over time of the vertical contact forces in the event that the driving wheelset has wheels in its new condition and is running on a track fitted with elastic rail plates, and Figure 12 shows the contact forces for the same driving wheelset but moving on a track with rigid rail plates.

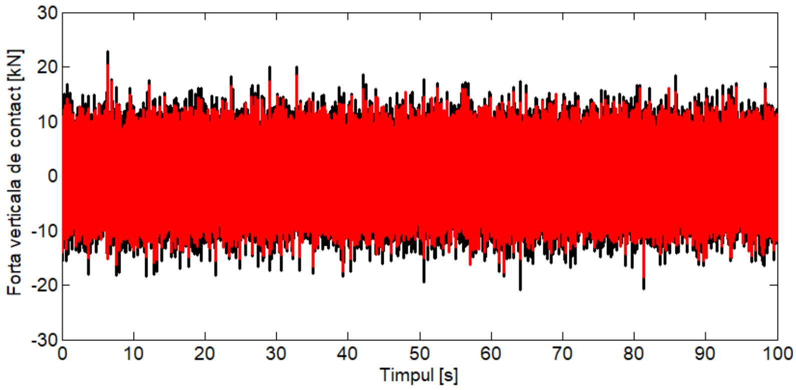

Fig. 12. Synthesis of vertical contact forces: wheels in the new state - track with rigid rail plates; —, wheel 1; —, wheel 2.

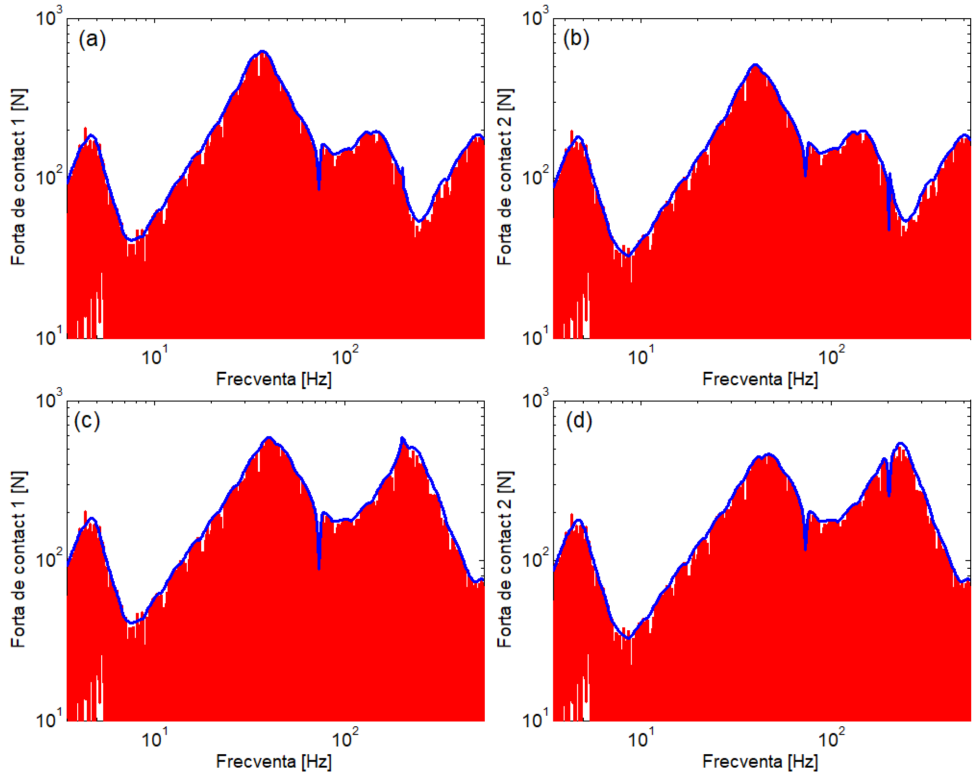

Fig. 13. Amplitude spectra of vertical contact forces (wheels in the new state): (a) wheel 1 – elastic wafers; (b) wheel 2 - elastic wafers; (c) wheel 1 - rigid plates; (d) wheel 2 – rigid plates; —, spectrum calculated on the basis of the sequence over time; ; —, spectrum resulting from frequency analysis.

The differences between the vertical contact forces acting on the two wheels shall be observed. In addition, the amplitude of vertical contact forces is higher in the case of running on a track with rigid rail plates, and this is in line with the results obtained from the analysis of the amplitude spectra presented above.

Figure 13 shows the amplitude spectra of the contact forces obtained by Fourier analysis of the time sequences shown in Figures 11 and 12. For verification, the amplitude spectra of vertical contact forces obtained from frequency analysis (see Fig. 10) are also presented. It is noted the good concordance between the results obtained by the two methods of calculation.

5. Study of longitudinal vibrations of the driving system of the driven wheelset

In this chapter is presented the model of longitudinal vibrations that develop in the drive system of the driving wheelset when a locomotive is running at the adhesion limit and the phenomena specific torsion and rebound vibrations are analyzed.

The longitudinal vibration model comprises the driving wheelset with the elastic driving system and the rotor of the electric traction motor, including the torsion shaft and the reducing gear through which the motor torque is transmitted to the wheelset wheels. The driving wheelset is driven by a three-phase asynchronous short-circuit rotor motor working in stationary mode. Thus, the supply voltage and its frequency are constant, and the torque applied to the rotor depends only on the sliding of the motor according to its mechanical characteristic. The interaction between the driving wheelset and the track is manifested at the level of contact between the wheels and the rails by the vertical contact forces that have been calculated with the model shown in Chapter 4, and by the frictional forces on the periphery of the wheels for which Polach's model was adopted.

The nonlinear equations of torsion and rebound vibrations of the driving wheelset and drive system, which manifest as disturbances in relation to the stationary regime, are inferred.

The stability of the stationary regime of the drive system of the driving wheelset corresponding to the nominal operating regime of the electric motor according to the locomotive's traction characteristic and in correlation with the variability of the friction coefficient between the wheels and the rails due to the state of the contact surfaces (dry/wet surfaces) is analyzed. For this, the nonlinear equations of the stationary regime are deduced to calculate the values of its state parameters (equilibrium position). Then the linearized equations that describe the small disturbances around the stationary regime are inferred in order to identify its stable configurations. Stable configurations are identified based on the calculation of eigenvalues of the matrix of linearized equations rewritten in the form of equations with ordinary derivatives of the first order. Continue with nonlinear stability analysis based on the Hopf fork diagram.

The regime of longitudinal vibrations induced by the variation of vertical contact forces caused by the presence of irregularities on the running surfaces is studied. The influence of the damping of the guide system and the elastic coupling between the torsion shaft and the reducer gear on the traction performance of the driving wheelset is emphasized.

5.1. Model of the longitudinal vibrations of the driven wheelset

Figure 14 shows the overall outline of the mechanical model of the driving wheelset and the drive system running at constant speed V on an straight and level track.

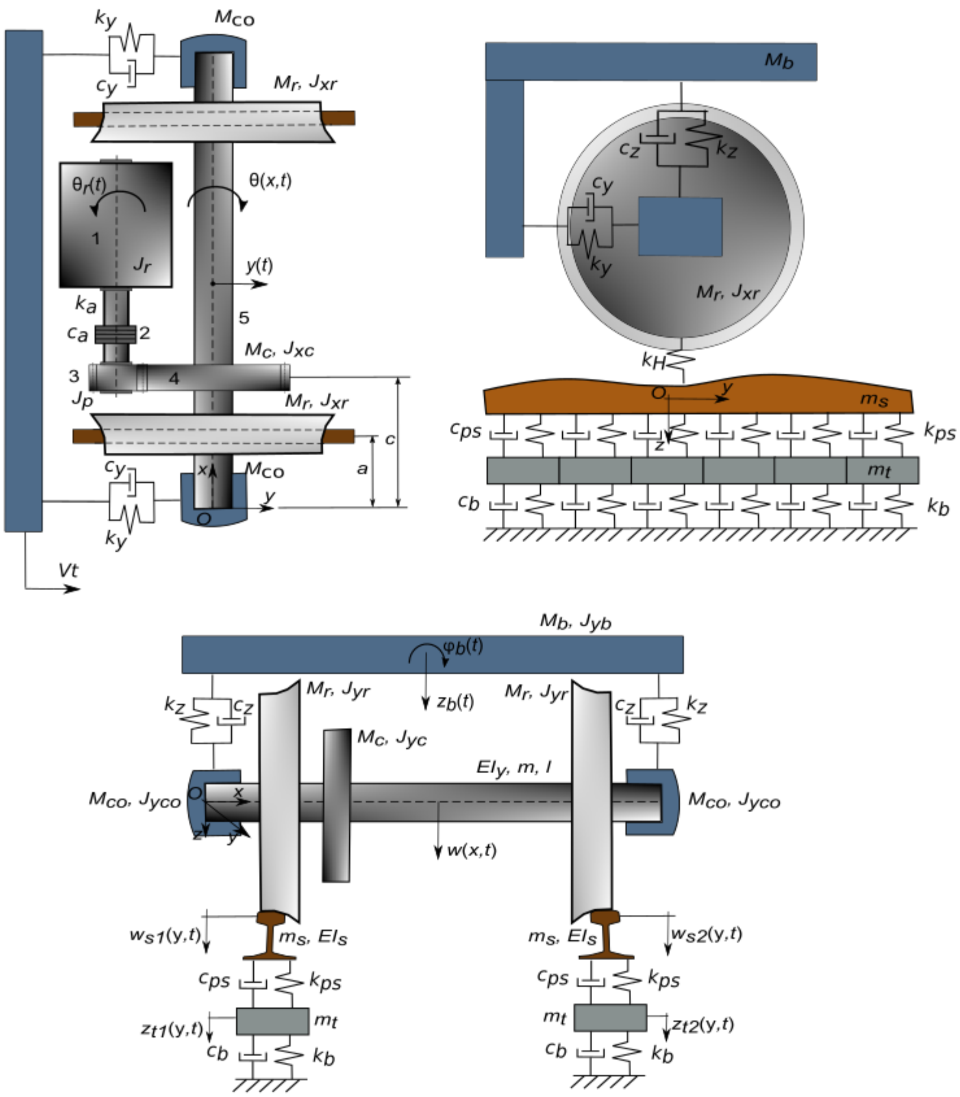

Fig. 14. Mechanical model of the interaction between the driving wheelset and the running track.

The drive system of the driving wheelset is of a one-sided type and consists of the rotor (1) of the electric traction motor which, by means of the assembly of the elastic shaft – coupling (2) and the reducer formed by the sprocket (3) and the toothed crown (4), transmits the motor torque C_m to the driving wheelset (5). The driving wheelset, which consists of the wheelset, wheels, wheelset boxes and geared crown, is driven elastically by a rigid movable base representing the chassis of the bogie and supports its part of the suspended mass by means of the primary suspension.

The running track is represented by the two rails, each working independently on a continuous foundation with two elastic layers and an intermediate inertial layer.

Vibration regim is manifested both in the form of vertical vibrations and in the form of longitudinal vibrations. Vertical vibrations are induced by tread irregularities, while longitudinal vibrations are generated, on the one hand, by variations in motor torque and, on the other hand, by variations in vertical contact forces. In other words, vertical vibrations are independent of longitudinal ones, while the latter are conditioned by vertical vibrations.

With the specification that the vertical vibration regime was treated in Chapter 4 resulting, inter alia, in vertical contact forces in the form of time functions, only the regime of longitudinal vibrations, namely the torsion and reboung vibrations of the driving wheelset and the actuator system, is still treated.

The driving wheelset model for torsion vibrations is identical to that shown in Chapter 3. The elastic guidance of the wheelset is shaped by a Kelvin-Voigt system. The rotor, sprocket and crown are shaped by rigid bodies in rotational motion, and the elastic shaft is represented by a torsional spring.

The parameters associated with torsion and rebound vibrations are: (a) the driving wheelset: the length of the wheelset l, the mass per unit of length equal to $m = \rho S$, where ρ is the density of the material and S represents the mean area of the cross-section of the wheelset, the rigidity at the GI_p torsion, in which G is the transverse modulus of elasticity, and I_p is the polar inertia moment of the cross-sectional middle section, the moment of axial inertia of the wheel J_{xr}, the moment of axial inertia of the toothed crown J_{xc}, the distance between the wheels and the ends of the wheelset a, the distance between the gears and the close end of the wheelset b, the distance between the wheels $2e$; (b) actuation system: moment of inertia of the rotor J_m, moment of inertia of the sprocket J_p, torsion stiffness of the elastic shaft assembly — coupling k_a and constant damping constant corresponding to c_a; (c) wheelset conduction system: k_y stiffness and damping constant c_y.

The following assumptions shall be adopted:

a) In the equilibrium position, the vertical contact forces are equal on the two wheels of the driving wheelset;
b) The influence of the electro-magnetic circuit of the motor on the motor torque is neglected – the motor works only according to its mechanical characteristic;
c) Frictional forces are calculated according to Polach's simplified relationships [based on Kalker's theory
d) The meandering motion of the driving wheelset is neglected because its frequency is much lower than the frequencies of longitudinal vibrations of torsion and rebound;
e) The effect of the secondary suspension is neglected, and the influence of the locomotive box is reduced to its weight for a similar reason to the one above;
f) The torsion vibration of the driving wheelset is reduced to the rigid vibration mode and the first two elastic modes;

g) The effect of the forces induced by the transmission of the motor torque on the load of the driving wheelset shall be neglected;
h) The wheelset load shall be considered not to be affected by the locomotive's bouncing;
i) Neglect losses in the traction gear.

The following are inferred the nonlinear equations of motion that describe the torsion vibrations of the drive system of the driving wheelset and the rebound vibrations of the driving wheelset connected by the elastic guiding system to the bogie frame. They depend on the motor torque applied to the rotor and the frictional forces on the periphery of the wheels that are calculated in the next two sections.

5.2. Motor torque

In this section is shown how to calculate the motor torque according to the angular velocity of the rotor of the electric traction motor for use in the model of longitudinal vibrations of the driving wheelset. The relationship between the motor torque and the angular velocity of the rotor defines the mechanical characteristic of the electric traction motor. The mechanical characteristic of the three-phase asynchronous motor is used.

5.3. Frictional forces

Considering that the normal contact force is approximately equal to the vertical contact force because the angle of contact between the wheel and the rail is small, the frictional forces acting on the two wheels can be calculated.

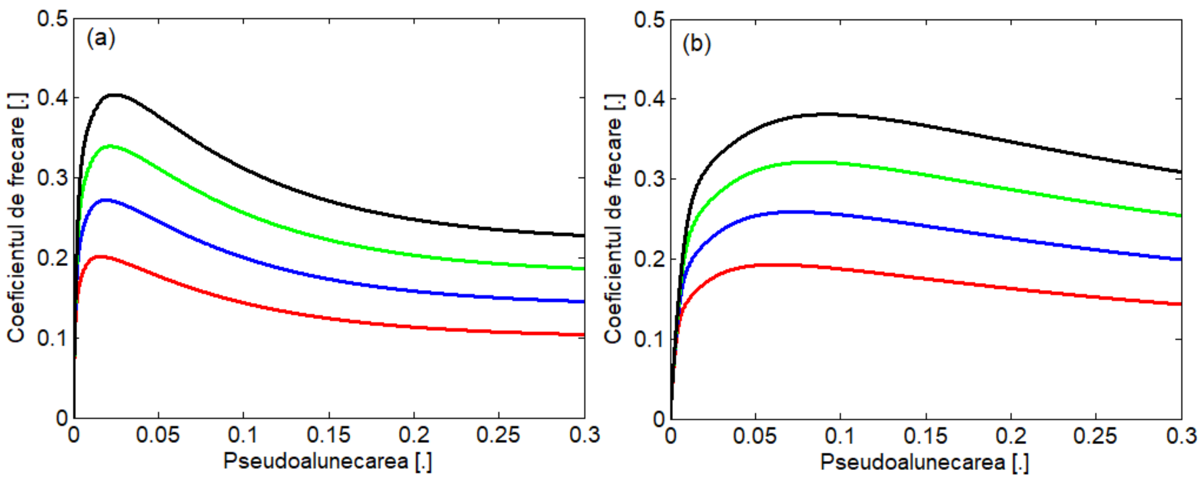

Fig. 15. Simulation of the variability of the wheel-rail friction coefficient: (a) dry surfaces; (b) wet surfaces; — *ms* = 0,25; — *ms* = 0,35, — *ms* = 0,45; — *ms* = 0,55, ms – static coefficient of friction.

Appling Polach's model which is recommended to be used in the dynamics of traction vehicles. This model has the advantage that it is simple to apply and offers good calculation accuracy. At the same time, the model allows to simulate the variability of the coefficient of friction between the wheels and the rails depending on the state of the treads (dry/wet) (fig. 15).

5.4. Stability of the stationary regime

The first stage of the analysis of the longitudinal vibrations of the drive system of the driving wheelset is aimed at calculating the values of the parameters of the stationary regime and determining its stability. The stationary regime is defined as the regime in which the state sizes do not vary over time except for the components that define the reference state. The drive system of the driving wheelset is stable if, in the absence of excitation factors, the free longitudinal vibrations associated with a particular stationary regime decrease over time. If, however, the free vibrations increase, then the system is unstable.

The issue of the stability of the drive system of the driving wheelset is very important for the proper functioning of the locomotive. The instability of the drive system of the driving wheelset is manifested in the form of stick-slip vibrations that induce variations in the traction force and high loads throughout the motor torque transmission chain, thus affecting the fatigue resistance of the entire system. Stick-slip vibrations cause wear of the treads of the wheels and rails, as well as wear of the traction gear.

From the nonlinear equations of motion are inferred the equations of the stationary regime which are nonlinear algebraic equations that can be solved by applying the Newton-Raphson method. Rewrite the nonlinear equations of motion so that they describe the perturbated motion around the stationary regime, and then proceed to their linearization.

Linear stability analysis is based on the calculation of the matrix values of the system of linearized motion equations rewritten in the form of first-order differential equations. Array eigenvalues can be complex-conjugated or real because matrix terms are real numbers. The stationary regime of the drive system of the driving wheelset is stable if all the eigenvalues have the negative real side – the system is *asymptotically stable*, and the amplitude of movement around the equilibrium position decreases continuously. If at least one natural value has the positive real part, then the system is *unstable*, and the amplitude of motion increases exponentially depending on time. At the limit, when a pair of complex-conjugated eigenvalues have no real part, the system is *simply stable*, the amplitude of the free oscillations is constant.

5.5. Solution of the nonlinear equations of the system drive of the driving wheelset

In this section is presented the method of solving the nonlinear equations of the drive system of the driving wheelset that describe the longitudinal vibrations associated with a particular stationary regime. The specific aspects of nonlinear vibrations which are investigated in the section reserved for longitudinal vibration analysis are also established.

The system of nonlinear equations may have as a solution the equilibrium position obtained from the equilibrium equation between the motor torque at the toothed crown and the torque of the frictional forces. This equilibrium position is the *stationary solution* of the equations of motion. If the stationary solution is not stable, then the movement of the drive system of the driving wheelset takes the form of periodic movement. In other words, nonlinear and homogeneous motion equations admit *periodic solutions* known as *limit cycles*. Identifying limit cycles that manifest themselves in the form of stick-slip vibrations is important because, as has been shown, they have unfavourable effects on the traction performance of the locomotive and on the fatigue resistance of the entire traction system.

Another interesting aspect from a theoretical and practical point of view is the study of the forced longitudinal vibrations of the drive system of the driving wheelset under the action of the vertical contact forces caused by the vertical interaction between the wheelset and the raceway. This type of excitation is of a parametric nature coming from the vertical interaction between the driving wheelset and the running track. The variation of the vertical forces leads to the variation of the frictional forces which thus induce a permanent regime of forced vibration. To study this vibrational regime, it is necessary that the vertical forces of contact wheel-rail, obtained on the basis of the model of the vertical interaction motor-track wheelset presented in the Chapter 4, to be introduced into the equations of the frictional forces.

5.6. Analysis of longitudinal vibrations

In this section, based on the model of interaction between the driving wheelset and the running track shown in Chapters 4 and 5, the numerical results regarding the longitudinal vibrations of the drive system of the driving wheelset of the driving wheelset are analyzed.

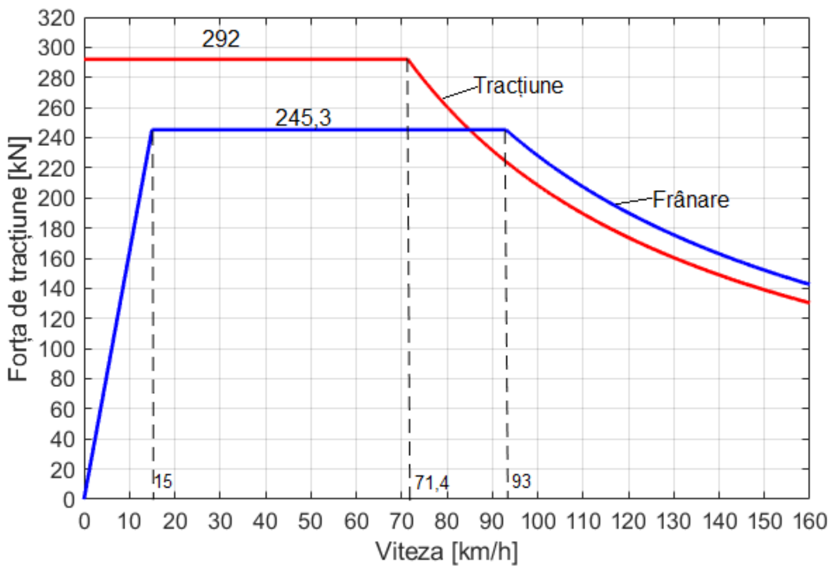

Fig. 16. The traction and braking limit characteristics of the LEMA locomotive.

The values of the numerical application correspond to the LEMA locomotive produced by SOFTRONIC from Craiova, which is equipped with asynchronous motor, whose traction characteristic is given in Figure 16. The speed limit is 71.4 km/h.

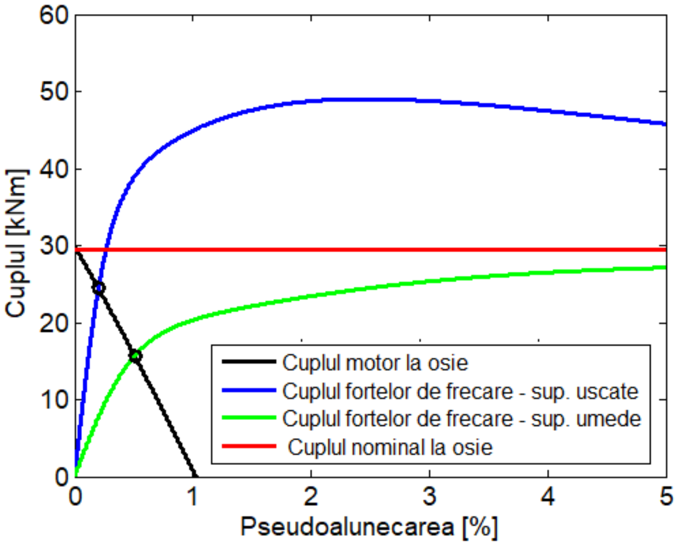

\

Fig. 17 Illustrative for determining the stationary regime at *V* = 71,4 km/h.

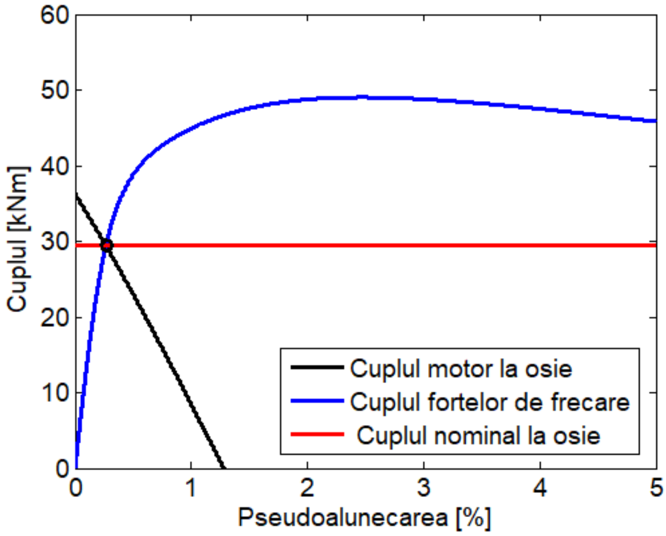

Fig. 18. Illustrative for determining the stationary regime at *V* = 71,224 km/h – dry running surfaces.

Figure 17 shows the stationary regime of the driving wheelset at rated speed when travelling on dry/wet treads. The stationary regime shall be determined according to the creepage when the motor torque at the wheelset is balanced by the torque of the frictional forces. The figure also shows the nominal value of the wheelset motor torque corresponding to the traction limit characteristic (red line). It is noted that it is not possible to achieve the nominal value of the motor torque regardless of the condition of the treads. The explanation lies in the fact that when calculating the traction characteristic of the locomotive, the ideal conditions regarding the movement of the driving wheelsets were considered ideal without taking into account the influence of the effect of the creepage on the motor slip. The timing of the drive wheelset, without which the wheelset cannot develop traction force, causes the motor slip to be reduced, which explains why the motor torque transmitted to the wheelset is lower than that obtained from the locomotive's traction characteristic.

In order to compensate for the decrease in motor slip due to creepage of the wheelset, it is necessary to decrease the rotational speed of the wheelset, that is, to reduce the speed of traveling. For example, Figure 18 shows the wheelset torque and the torque of the frictional forces in the case of dry running surfaces depending on the wheelset's creepage at a speed of 71,224 km/h which is less than the nominal value.

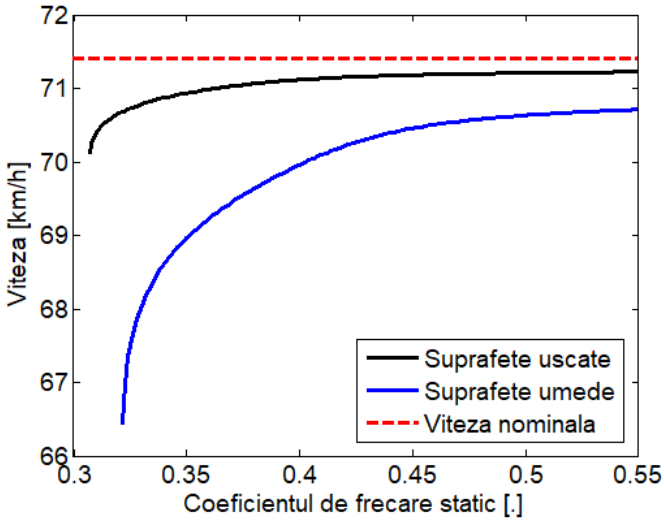

Fig. 19 Running speed at rated torque.

Of course, this deviation of the speed of the nominal regime in relation to the ideal one (71.4 km/h) is insignificant. Figure 19, however, shows what happens if the wheel-rail friction coefficient takes values throughout the range shown in Figure 15. In the figure mentioned is represented the running speed at which the torque developed by the motor takes the nominal value according to different values of the wheel-rail static friction coefficient; it is recalled that the variability of the coefficient of friction is obtained by modifying the coefficient of static friction. The motor torque at the wheelset takes the nominal value at ever lower speeds if the static wheel-rail friction coefficient decreases and thus reaches the adhesion limit. In the case of dry running surfaces, the speed at which the nominal wheelset torque can be obtained decreases from 71,224 km/h for the maximum value of the wheel-rail static friction coefficient (to be obtained for m_{μ}= 0,55) to 70,091 km/h corresponding to the adhesion limit (m_{μ} = 0,307). If the treads are wet, then speed reductions are much more important.

The driving wheelset converts the motor torque into traction force and the rotational movement into translational motion. The traction force occurs as a result of friction between the wheels and the rails due to the creepage effect of the wheelset on the track, and for this reason the conversion of the motor torque into traction force is made on account of the losses that occur. The mechanical effectiveness of the wheelset is reflected in its efficiency defined as the ratio of useful power to the power consumed.

For a given stationary regime, the efficiency of the driving wheelset depends solely on the creepage corresponding to that stationary regime in the sense that the reduction in efficiency is equal to the increase in creepage. As the size of the creepage depends on the condition of the treads, being larger if the treads are wet, it follows that for these conditions the efficiency of the driving wheelset is affected. At the same time, the efficiency decreases as the adhesion conditions worsen, respectively the wheelset approaches the adhesion limit (fig. 20).

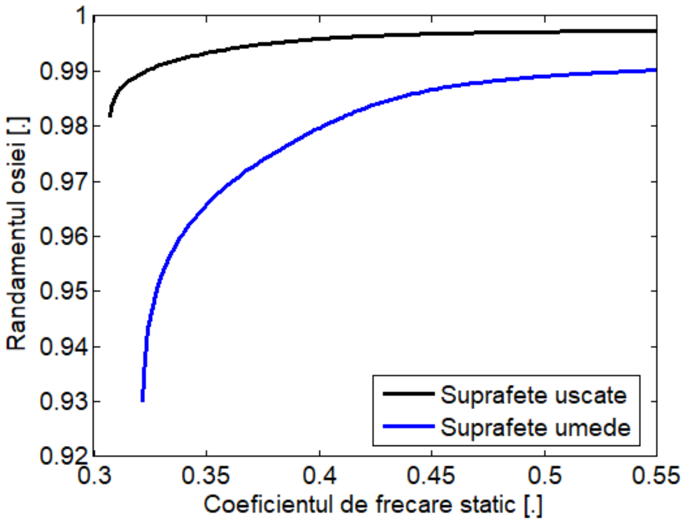

Fig. 20. Wheelset efficiency.

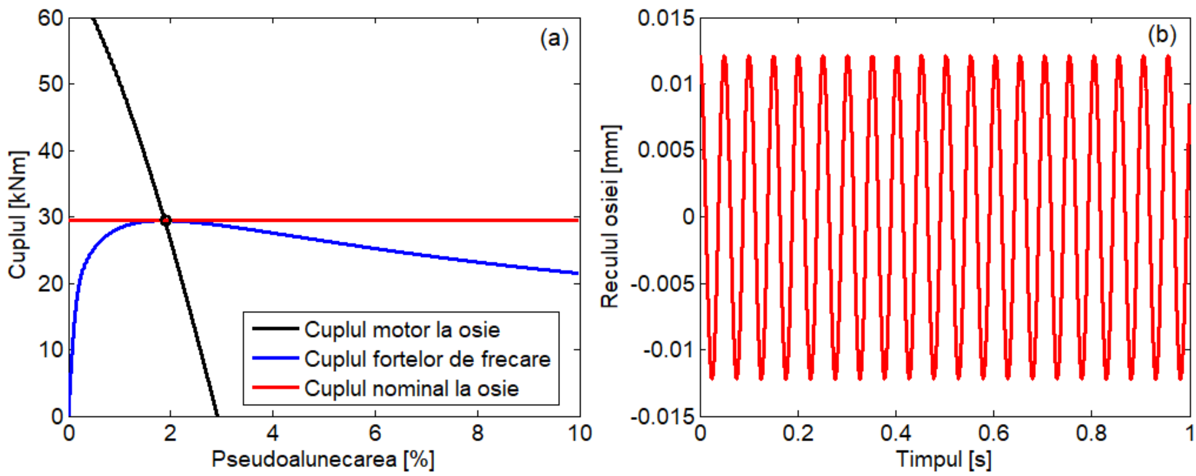

Fig. 21. Stability of the stationary regime at the adhesion limit to *V* = 70,10097 km/h and m_μ = 0,307365 (dry surfaces): (a) stationary regime; (b) wheelset recoil.

The linear stability analysis shows that, neglecting the damping of the elastic coupling between the torsion shaft and the reducing gear, as well as the damping of the wheelset driving system, at the adhesion limit, the driving wheelset is at the stability limit, regardless of whether the treads are dry (fig. 21) or wet (fig. 22); the regime at the adhesion limit is simply stable. Under the same damping conditions, the stationary regimes located on the ascending (stable) branch of the friction force curve as a function of the sliding rate (see Fig. 23) are asymptotically stable (Fig. 24 for dry surfaces and fig. 25 for wet surfaces), and those on the descending branch (unstable) are unstable (fig. 26). The stable/unstable character of the stationary regimes is explained by the contribution of the dynamic component of the friction force that may introduce positive or negative damping depending on the branch on which the stationary regime is located (see Fig. 23).

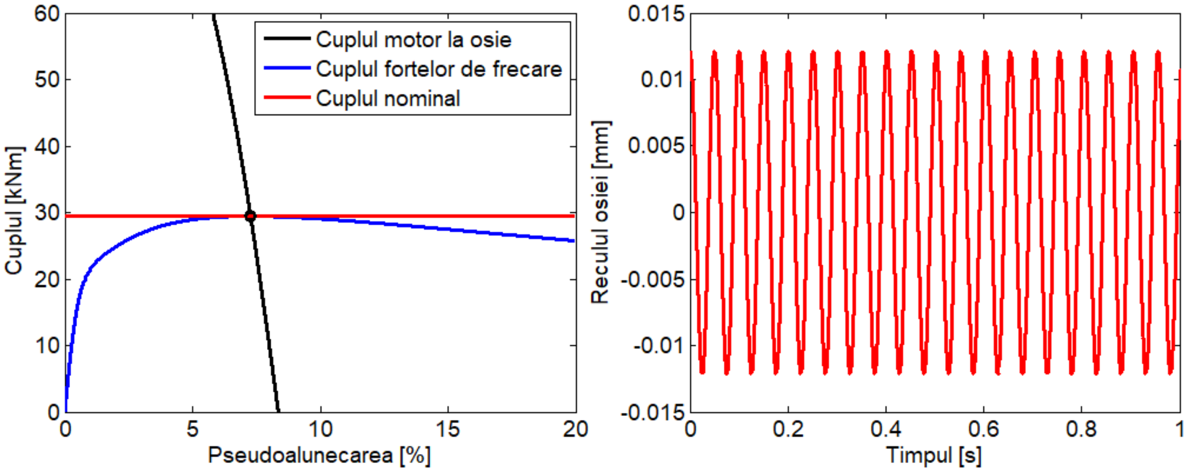

Fig. 22. Stability of the stationary regime at the limit of adhesion to *V* = 66, 56882 km/h and m_μ = 0,32173 (wet surfaces): (a) the stationary regime; (b) wheelset recoil.

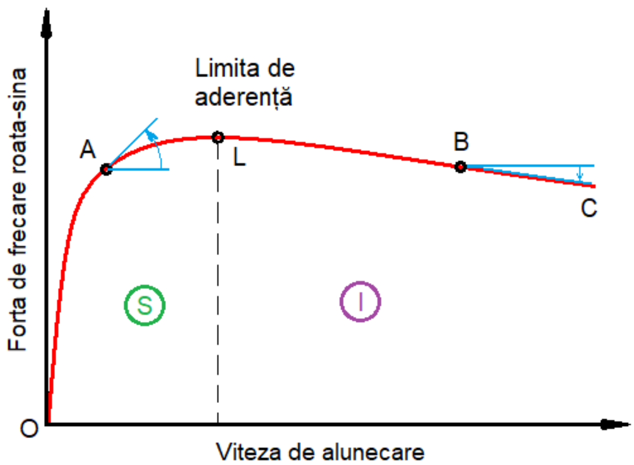

Fig. 23. Explanatory concerning the variation of the frictional force as a function of the wheel-rail sliding speed.

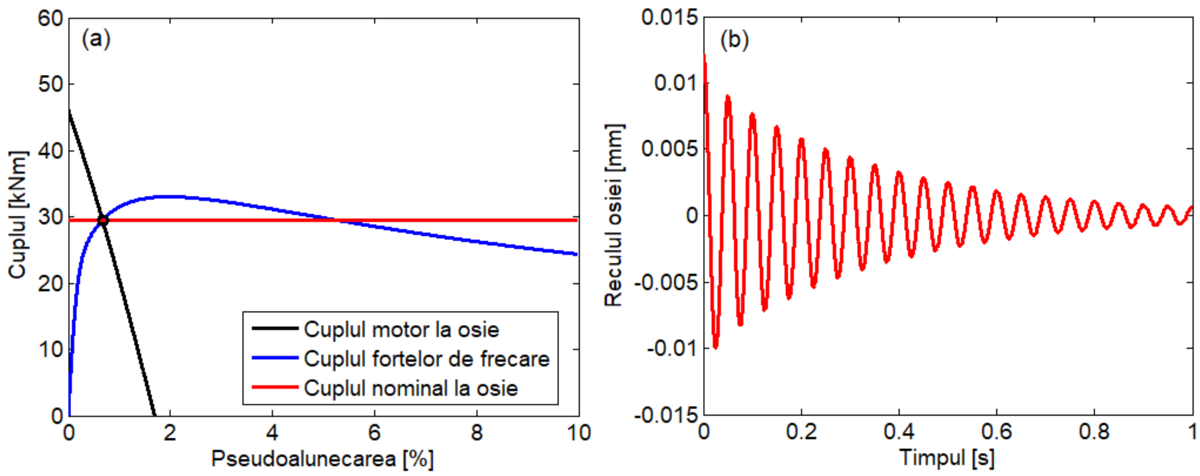

Fig. 24. Stability of the stationary regime at *V* = 70,9328 km/h and m_μ = 0,35 (on dry surfaces):

(a) the stationary regime; (b) wheelset recoil.

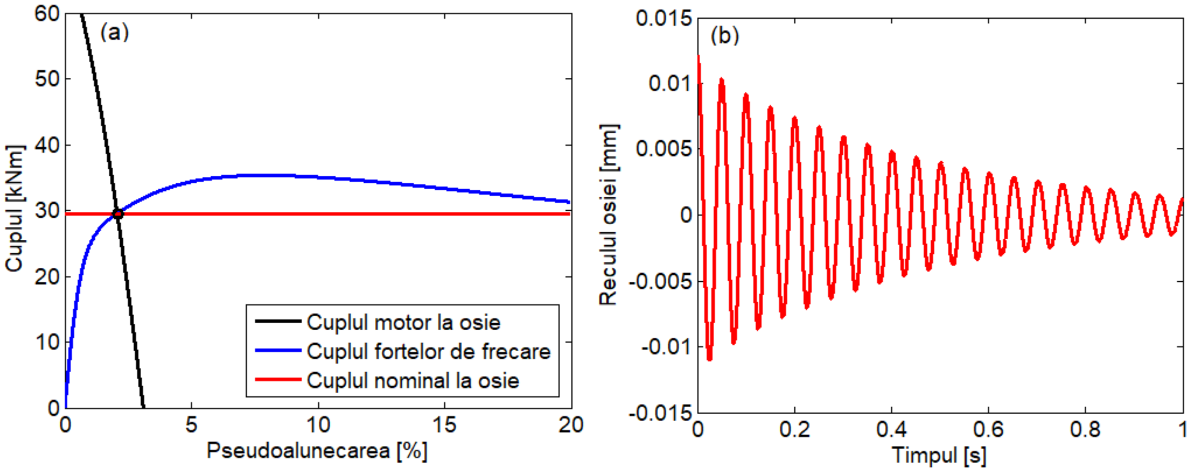

Fig. 25. Stability of the stationary regime at V = 69,9613 km/h and m_{μ} = 0,40 (wet surfaces): (a) the stationary regime; (b) wheelset recoil.

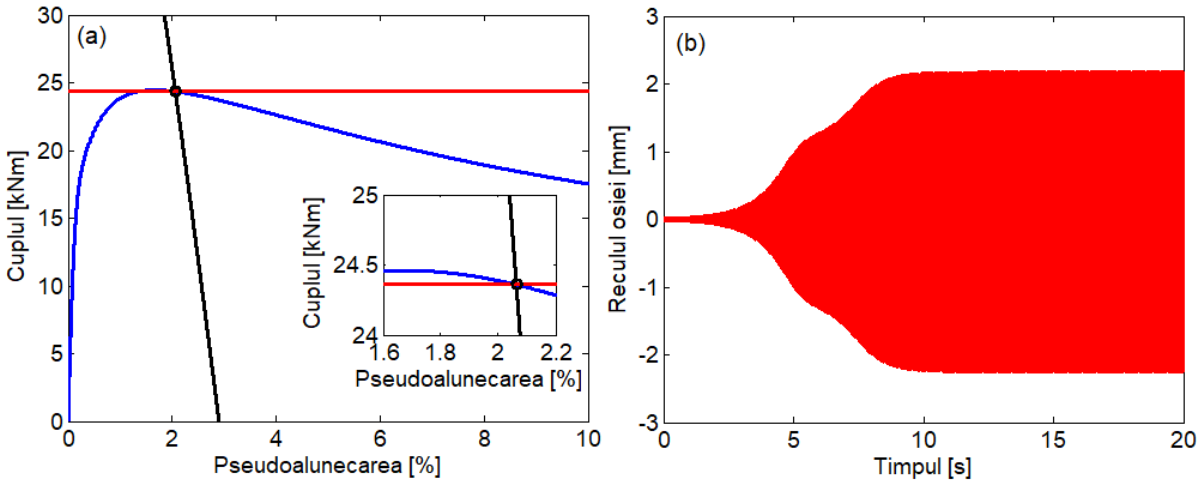

Fig. 26. Stationary regime when the adhesion limit is exceeded and the limit cycle at V = 70,10097 km/h and m_{μ} = 0,25 (dry surfaces): (a) stationary regime: -, motor torque at wheelset; - torque of the frictional forces, - actual torque, (b) limit cycle (initial recoil 1%·yo).

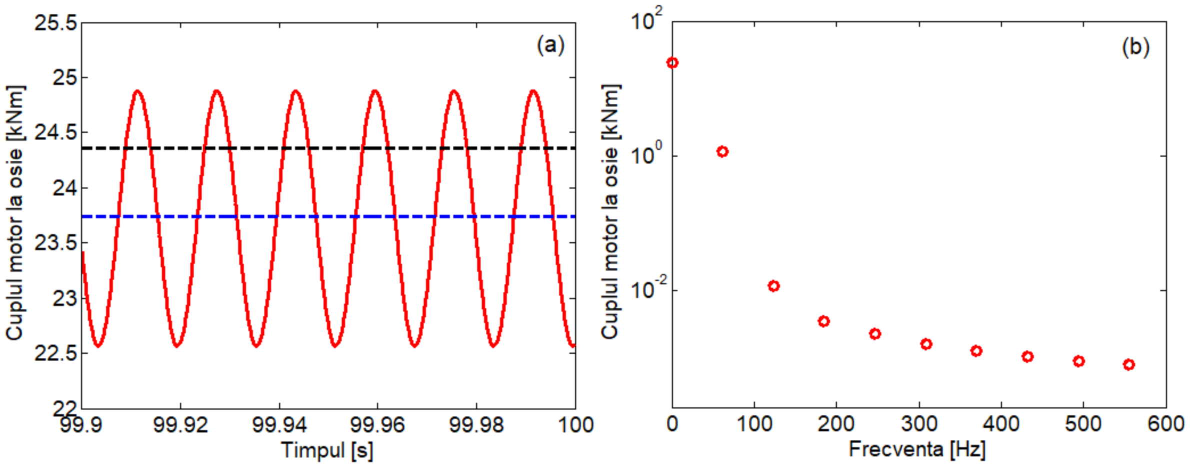

Fig. 27. Wheelset motor torque – torsion limit cycle: (a) variation over time; (b) the spectrum of amplitude; - instantaneous value, - value, mean value, mean value, stationary value.

The analysis of the nonlinear stability of the unstable stationary regimes (located on the unstable branch) showed that, in the absence of any depreciation, two stable limit cycles called torsion and rebound limit cycles are possible.

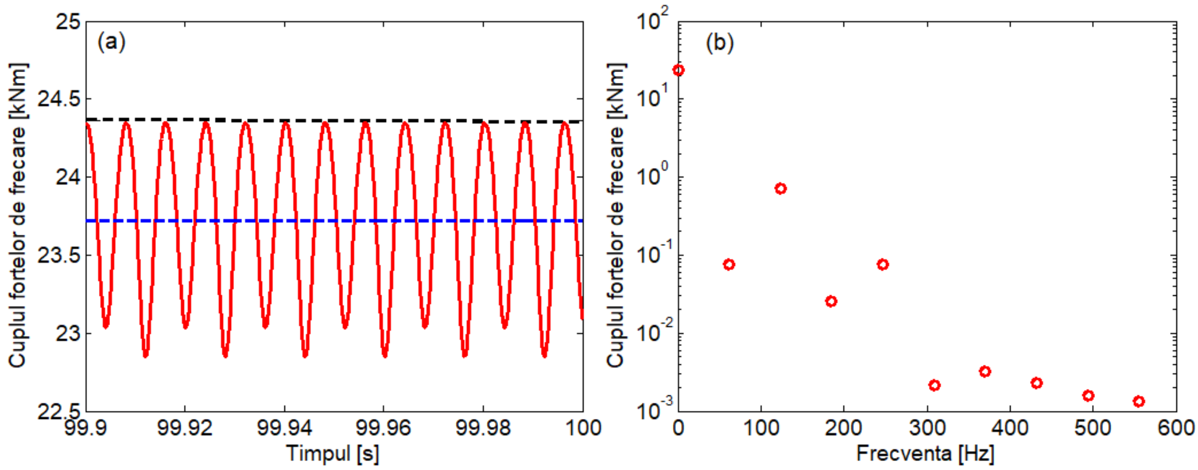

Fig. 28 Torque of frictional forces – limit cycle of torsion: (a) variation over time; (b) the spectrum of amplitude; - instantaneous value/amplitude, - mean value, mean value, mean value, stationary value.

The limit cycle of torsion is the frequency close to the resonance frequency of the first elastic torsion mode of the driving wheelset. It is characterized by the fact that it is accompanied by significant armonic components of the motor torque (fig. 27) and of the torque of the frictional forces (fig. 28) that may affect the mechanical strength of the wheelset.

The rebound limit cycle develops practically at the resonant frequency of the rebound movement of the wheelset connected by the elastic guiding system to the bogie frame and is manifested by very large oscillations of the traction force (fig. 29); the static load on the wheel is 100 kN.

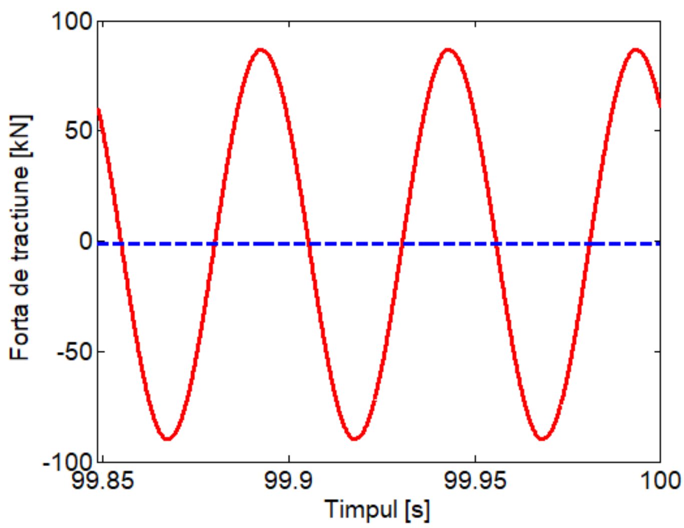

Fig. 29 Variation of the traction force - the limit cycle of rebound;
- the instantaneous value, - the mean value.

The existance of limit cycles is justified by the fact that an energy balance is reached between the accumulated energy and that dissipated during a period of the dynamic component of the frictional force which has a negative or positive dampening effect depending on the branch of the friction force curve on which it works.

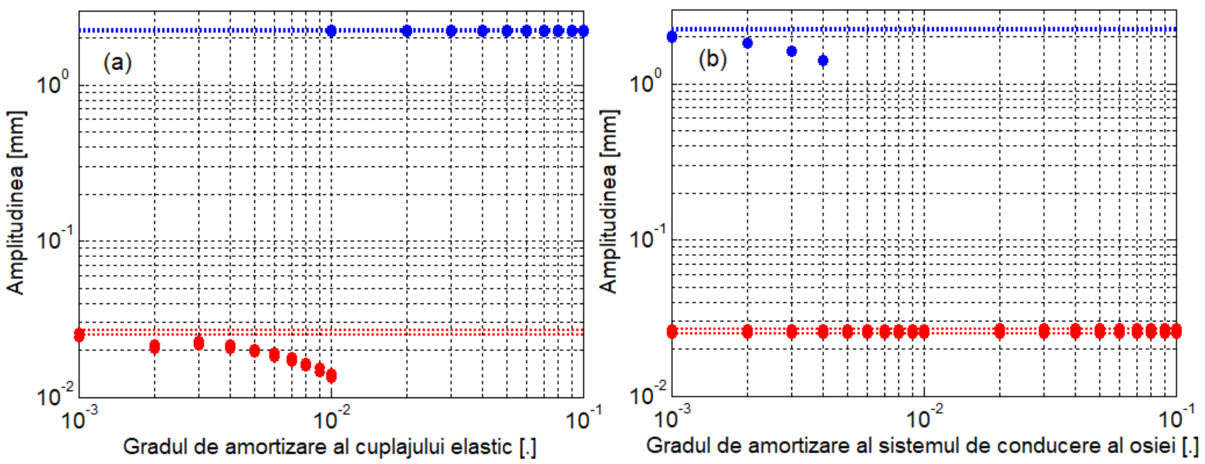

Fig. 30. Hopf bifurcation: (a) the degree of damping of the elastic coupling; (b) the degree of depreciation of the wheelset gui system; torsion limit cycle: ·······, without damping, •, with damping; the rebound limit cycle: ·······, without depreciation, •, with depreciation.

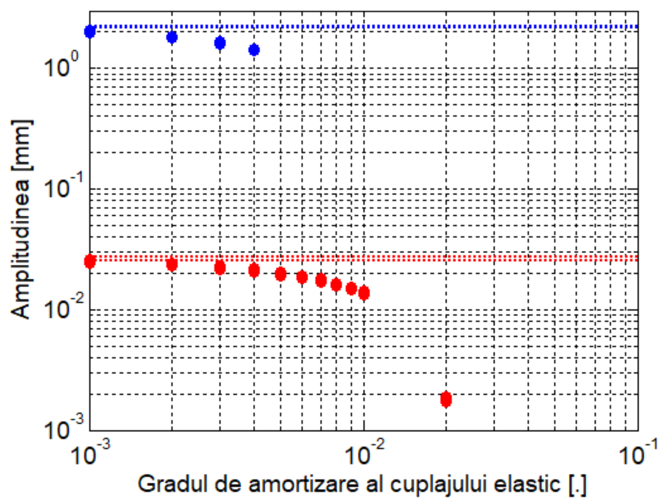

Fig. 31. Hopf bifurcation for equal degrees of damping; torsion limit cycle: ·······, without damping, •, with damping; the rebound limit cycle: ·······, without depreciation, •, with depreciation.

The damping of the elastic coupling or that of the wheelset steering system limits the areas in which the limit cycles may exist as shown by the Hopf bifurcation diagrams in Figure 30. In diagram (a), the configuration of the bifurcation according to the damping degree of the elastic coupling is shown, the damping of the wheelset guidance system being zero, while in diagram (b), the Hopf diagram is constructed for several values of the damping degree of the wheelset conduction system, neglecting the damping from the elastic coupling. The two diagrams contain the limits of the limit cycles calculated for the undamped system. The bifurcation point of the Hopf diagram having as its parameter the damping of the elastic coupling corresponds to the value 0,01 according to which the evolution of the wheelset drive system can take either the form of the rebound limit cycle or the shape of the limit cycle of torsion (diagram (a)). At lower values of the degree of damping of the elastic coupling, the limit cycle of rebound does not develop, and at higher values, the limit cycle of torsion disappears. The Hopf diagram according to the damping of the wheelset guidance system looks different (diagram (b)), in the sense that over the entire range of values investigated, it is possible to have the limit cycle of torsion, but the limit cycle of rebounds occurs only at low depreciation values.

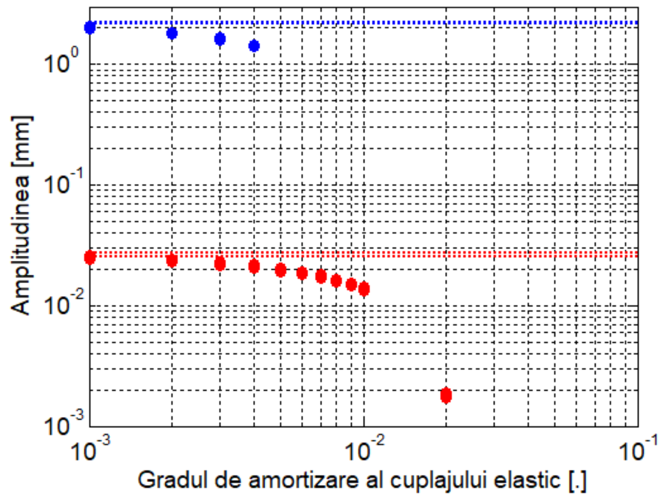

Fig. 32. Hopf bifurcation for equal degrees of damping; torsion limit cycle: ·······, without damping, •, with damping; the rebound limit cycle: ·······, without depreciation, •, with depreciation.

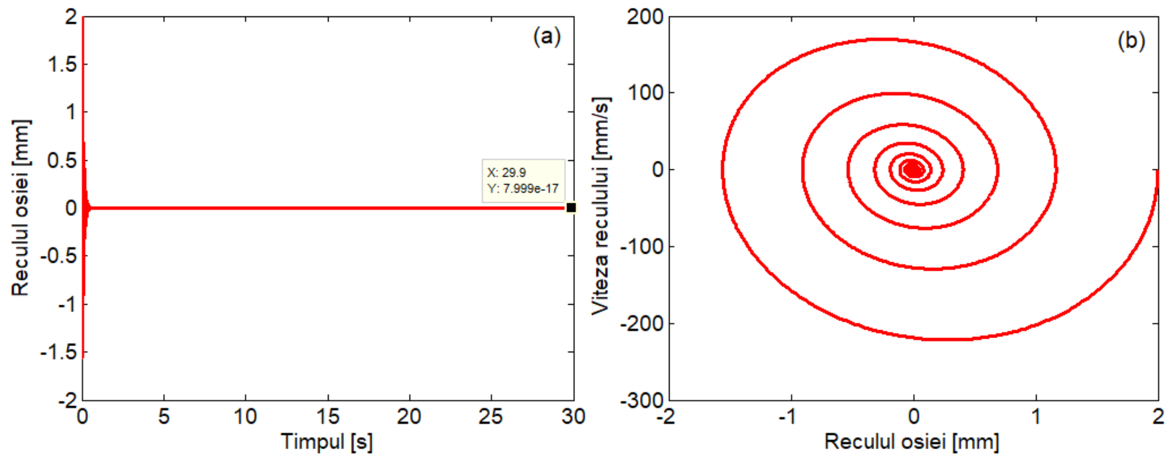

Fig. 33 Demonstrative for stable asymptotic stationary regime (damping degrees 0,1):
(a) wheelset rebound; (b) the trajectory of the phase.

Moreover, if the wheelset drive system and the driving system are properly depreciated, then the unstable stationary regime becomes asymptotically stable (v. fig. 32 and 33). Figure 32 shows the Hopf diagram considering the degrees of damping equal to 0,1. It is observed that the limit cycle of rebound occurs at low degrees of damping, while the limit cycle of torsion has a much wider range. Figure 33 shows the evolution of the rebound of the driving wheelset in relation to the stationary regime over a time sequence of 30 s. It is noted that rebound tends to the null value, which signifies the asymptotic stable character of the system.

The last stage of the analysis of the longitudinal vibrations of the wheelset drive system concerns the regime of forced vibrations due to the variation of the vertical forces of contact wheel-rail as a result of the vertical interaction between the driving wheelset and the track. The variation of the vertical contact force changes the dynamic component of the frictional force respectively the component which, depending on the sliding speed between the wheel and the rail, generates positive or negative damping. Due to this aspect, the excitation caused by the variation of the vertical force is an excitation of a parametric type.

It's interested in what happens in the grip boundary area when the motor is working at rated torque or close values. Therefore, the stationary regime analyzed above is considered when the variation of the vertical contact forces are those resulting in the case of rigid rail plates; the degree of damping is equal to 0,1 for the elastic coupling and the wheelset guidance system.

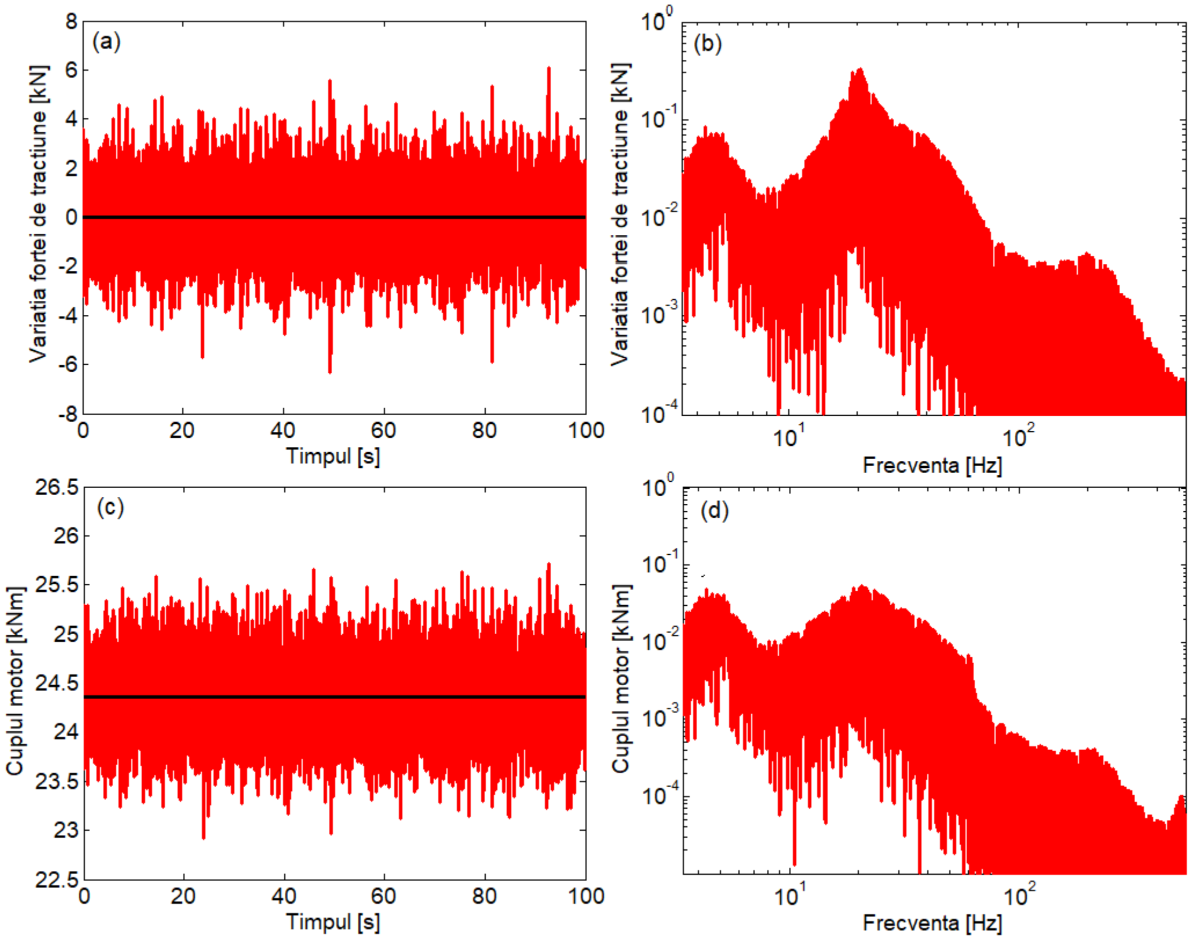

Fig. 34. Variation of traction force and motor torque when driving on a track with rigid rail plates (damping degrees 0,1): (a) variation in traction force; (b) the amplitude spectrum of the change in the tractive force; (c) the motor torque at the wheelset; (d) the amplitude spectrum of the motor torque at the wheelset.

Figures 34 and 35 show the variation in the tractive force, the motor torque at the wheelset and the evolution of the frictional forces on the two wheels, as well as the amplitude spectra of these dimensions. The variation in the tractive force oscillates around the null, which signifies that the average traction takes the value corresponding to the stationary regime. This is corroborated by the fact that the average of the wheelset motor torque also corresponds to the value of the stationary regime (24.36 kNm). The effective values of the variation of the traction force and the motor torque at the wheelset are: 1,337 kN and 0,351 kNm, respectively. The amplitude spectra of the variation in traction force and motor torque at the wheelset are dominated by 3 vertices. The most important is around the frequency of 20 Hz, a field in which the natural frequency of rebound motion (19.8 Hz) and the natural frequency of the rotor and elastic shaft system coupled with the driving wheelset (22.5 Hz). In the field of low frequencies, the vibration is dominated by the bouncing and pitch of the suspended part of the bogie (4-5 Hz), while at high frequency, a local maximum of the frequency spectrum occurs at more than 200 Hz due to the anti-resonance regime of the rail which determines a peak in the amplitude spectrum of the vertical contact force.

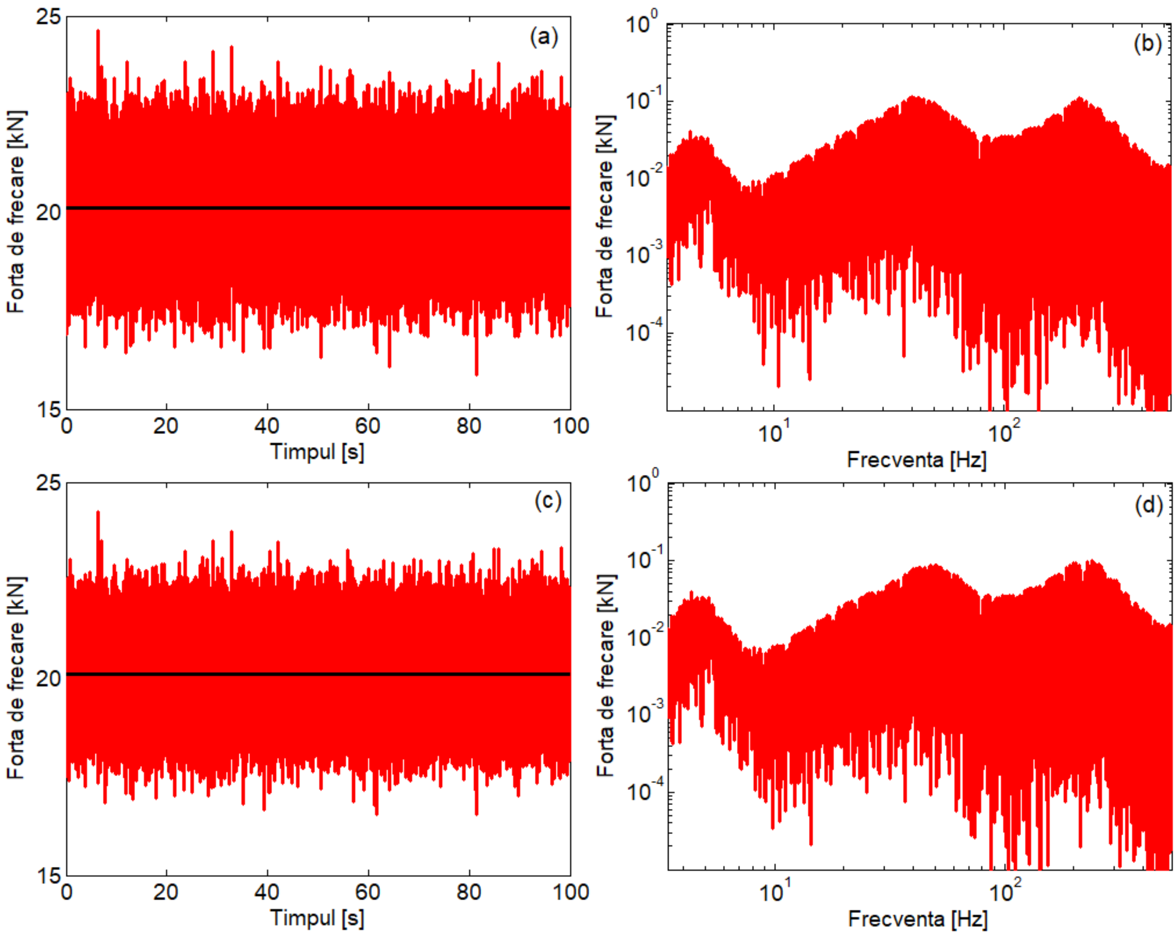

Fig. 35. Frictional forces when running on a track with rigid rail plates (damping degrees, 0,1): (a) on wheel 1; (b) the spectrum of amplitude; (c) on wheel 2; (d) the spectrum of amplitude.

The frictional forces on the periphery of the two wheels have practically the same average value, but the effective values are different, higher on the wheel 1, 0,914 kN, and lower on the wheel 2, 0,800 kN. The amplitude spectrum of the frictional forces reproduces at scale the amplitude spectrum of vertical contact forces (see Fig. 13, § 4). Thus, there are the maximums due to the bouncing and pitch of the suspended mass of the bogie (4-5 Hz), the resonance of the rigid vibration mode of the wheelset on the track (ca. 40 Hz) and the rail anti-resonance regime (approx. 200 Hz).

The fact that no peak is observed next to the natural frequency of the first wheelset torsion mode, but instead the peaks resulting from the vertical interaction between the driving wheelset and the running track are found shows that the differences between the frictional forces on the periphery of the two wheels are due to the vertical inertia asymmetry of the wheelset and not because of the inertial asymmetry of the wheelset at the torsion.

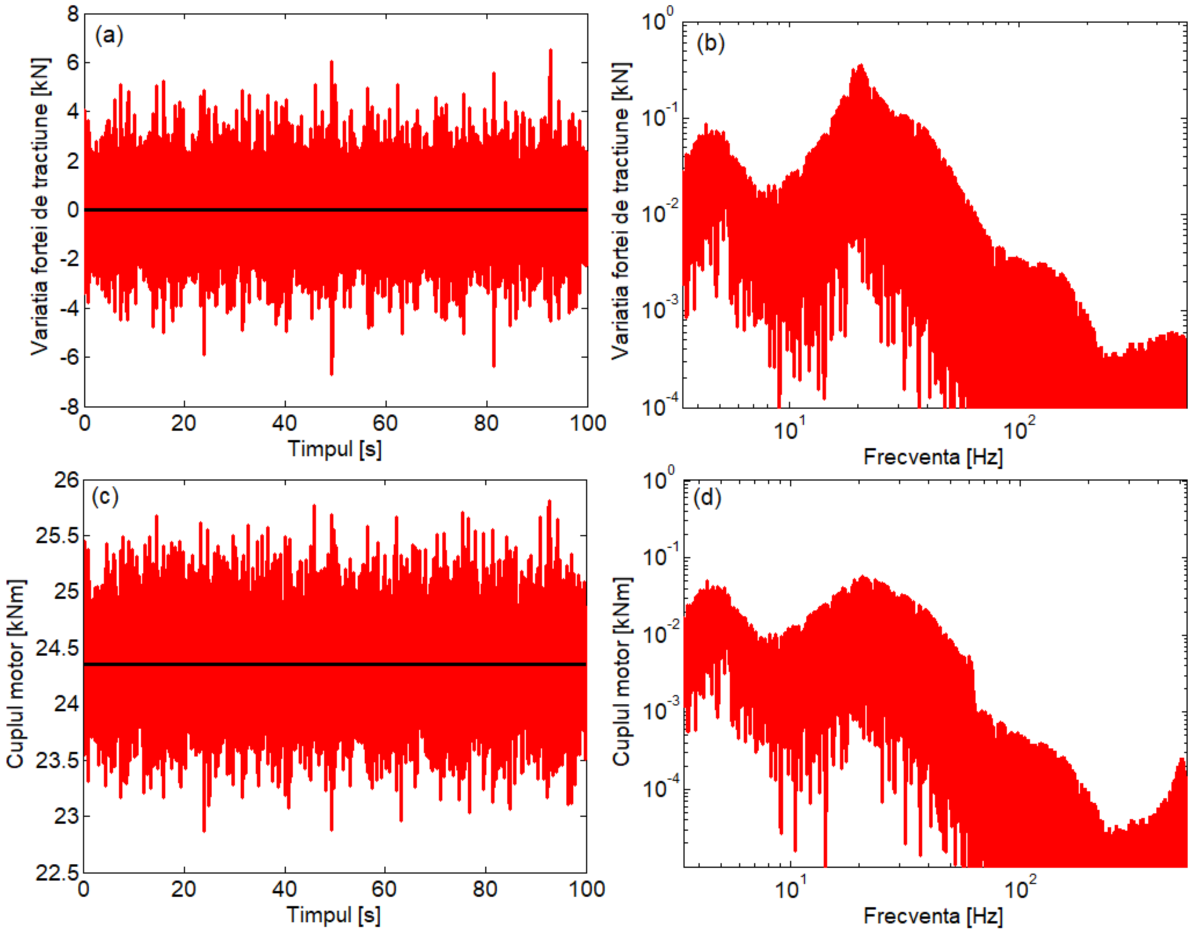

Fig. 36. Variation of traction force and motor torque when driving on a track with elastic rail plates (damping grades 0,1): (a) variation of the tractive force; (b) the amplitude spectrum of the change in the tractive force; (c) the motor torque at the wheelset; (d) the amplitude spectrum of the motor torque at the wheelset.

Figures 36 and 37 show the results of numerical simulations in case the wheelset runs on a track with elastic rail plates. It is recalled that obtained in Chapter 4, namely that the variation of the vertical contact forces is smaller compared to the situation where the rail plates are rigid. However, the effective value of the change in traction force (diagram (a) fig. 34) is greater than the value calculated when running the driving wheelset on the track with rigid rail pads, respectively 1,445 kN compared to 1,337 kN. And as for the motor torque at the wheelset (diagram (c) fig. 36), the same situation is observed, the effective value is 0.374 kNm compared to 0.351 kNm. Of course, the differences are not great, but apparently the results are contradictory.

The amplitude spectra of the variation of the traction force and of the motor torque at the wheelset (diagrams (b) and (c), fig. 37) are similar to those obtained in the previous case, with the difference that this time the local peak at about 200 Hz no longer appears, but attenuation of the fall of the spectral amplitude occurs at the frequency of 150 Hz corresponding to the anti-resonance of the rail when it has elastic pads.

Unlike the variation in traction force and motor torque at the wheelset, the frictional forces on the periphery of the wheels show lower effective values than those obtained in the case of rigid rail pads (diagrams (a) and (c), fig. 37). At the first wheel, the effective frictional force is 0,755 kN compared to 0,914 kN as it resulted in the case of the path with rigid rail pads, and on the second wheel, the effective value of the frictional force is 0,634 kN compared to 0,800 kN.

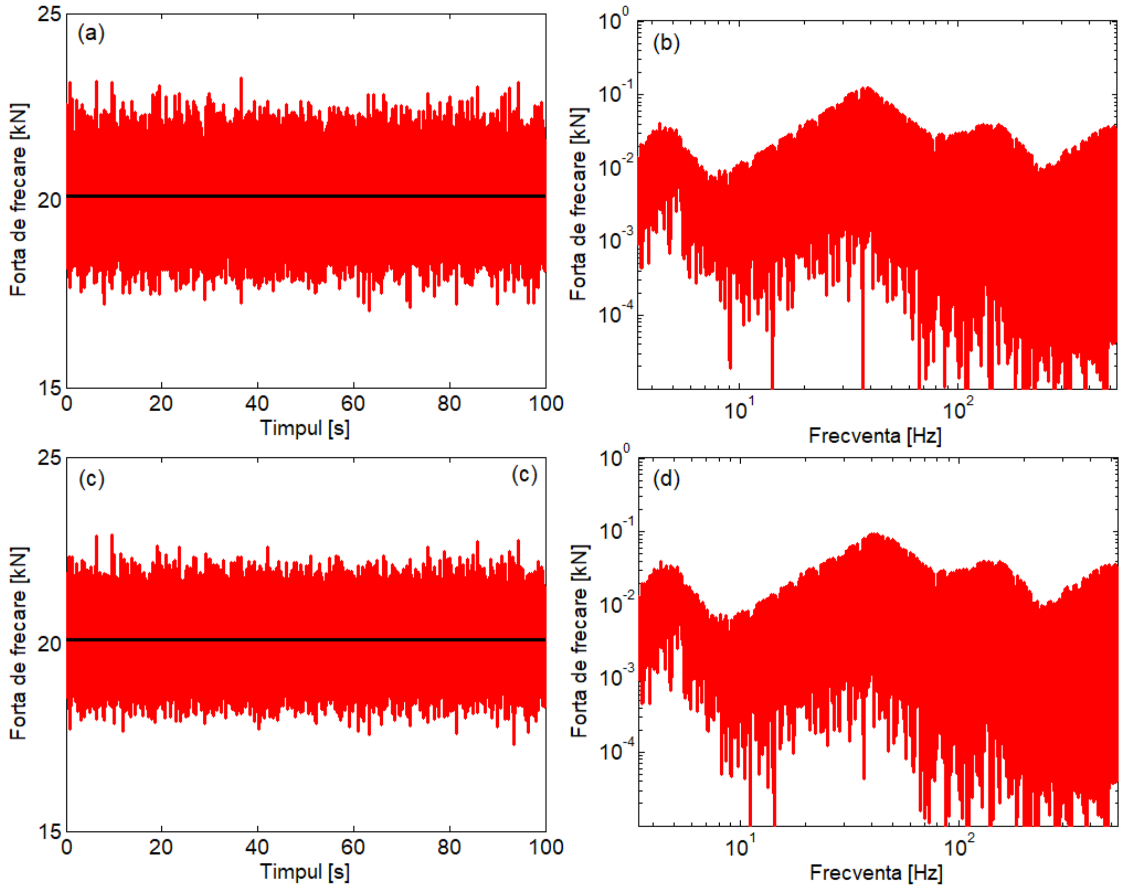

Fig. 37. Frictional forces when running on a track with elastic rail plates (damping degrees, 0,1): (a) at wheel 1; (b) the spectrum of amplitude; (c) on wheel 2; (d) the spectrum of amplitude.

The amplitude spectra of the frictional forces (diagrams (b) and (c) shown in Fig. 54) have maximum values corresponding to the bouncing-pitch frequency of the suspended mass of the bogie (4-5 Hz), the resonance frequency of the rigid vibration mode of the track wheelset (approx. 36 Hz) and the rail anti-resonance frequency (approx. 150 Hz).

It is therefore noted that the resonance frequency of the rigid vibration mode of the wheelset is lower than in the case of rigid rail plates and is therefore closer to the natural frequency of wheelset rebound. As a result, the effectiveness with which the frictional forces excite the rebound of the wheelset is higher, which explains why, despite the fact that the frictional forces are smaller, the variation in the traction force has a higher effective value as shown above.

The difference between the natural frequencies of rebound vibration and that of the rigid mode of vibration of the drive wheelset on the track for the longitudinal vibration of the driving wheelset is very important. To illustrate this, simulate the traction mode of the wheelset taking for rigidity of the wheelset conduction system the value *ky* = 60 kN/m. In this way, the rebound vibration's natural frequency reaches 34,4 Hz. For the rail pads, the stiffness corresponding to the elastic type plates is adopted.

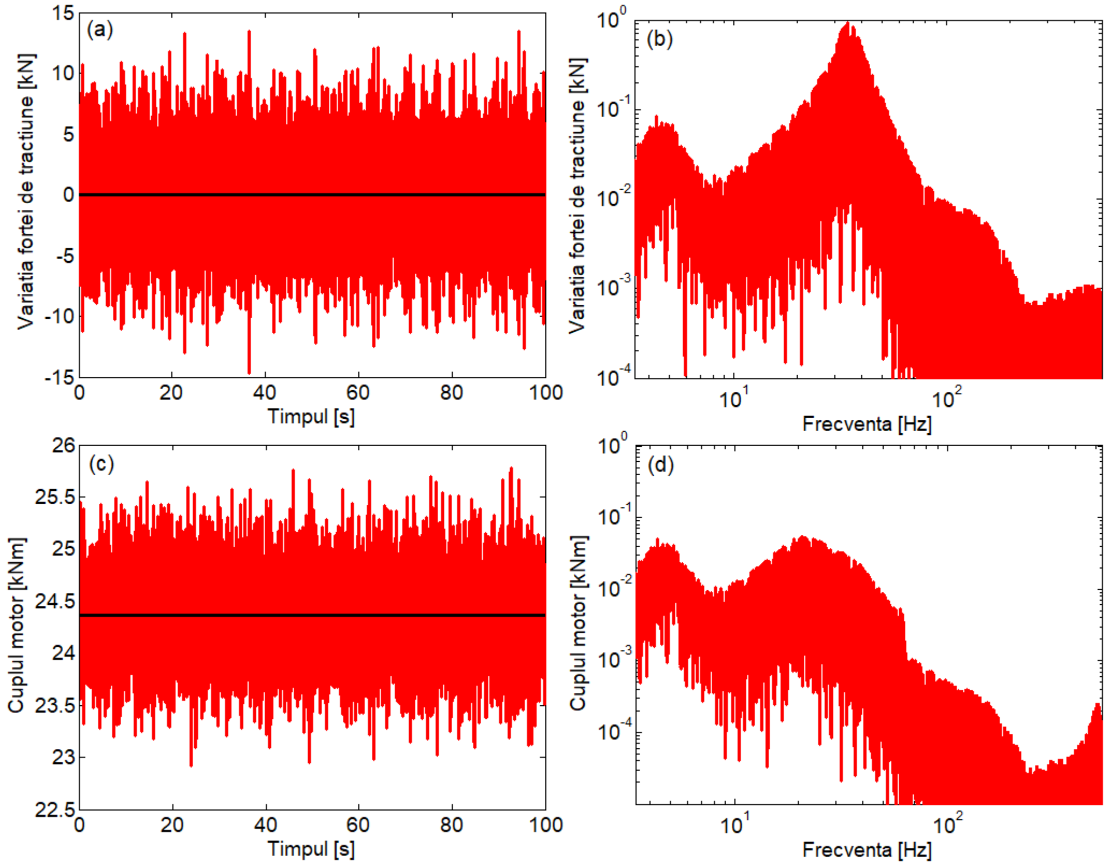

Fig. 38. Variation of traction force and motor torque when driving on a track with elastic rail pads (damping grades 0,1 and *ky* = 60 kN/m): (a) variation in traction force; (b) the amplitude spectrum of the change in the tractive force; (c) the motor torque at the wheelset; (d) the amplitude spectrum of the motor torque at the wheelset.

Figures 38 show the results of the numerical calculation for this case. Variation of the tractive force (diagram (a), fig. 38) reaches amplitudes of almost 15 kN, a value much higher than the amplitudes encountered in previous cases. The effective value of the change in traction force is also higher than the effective value obtained in the basic variant, namely 3,468 kN. The amplitude spectrum of the traction force variation is dominated by the amplitude resonance at ca. 36 Hz (diagram (b), fig. 38). Comparing the amplitude spectrum with that in the diagram

(b) of the fig. 36, it is observed, on the one hand, the displacement of the frequency as a result of the stiffening of the driving system of the driving wheelset, and on the other hand, the increase in amplitude as a result of the proximity to its natural frequency of the rigid mode of vibration of the wheelset on the track.

It is interesting that the stiffening of the wheelset steering system is practically without effect on the motor torque at the wheelset, as seen from the diagrams (c) and (d) of fig. 38 and the corresponding ones of fig. 36. The effective value of the motor torque is very close to what was obtained in the basic variant, 0.369 kNm compared to 0.374 kNm. There are no changes in the spectrum of motor torque either. The resonance of amplitude from ca. 20 Hz indicates under these conditions the connection between the variation in motor torque and the resonance frequency of the rotor and elastic shaft coupled with the wheelset by means of the gear.

It is important to know the characteristics of forced longitudinal vibrations when the stationary regime is on the ascending (stable) branch of the friction force curve depending on the wheel-rail sliding speed. Figure 39 shows the variation in traction force and motor torque when the driving wheelset develops the rated torque (29,443 kNm) when running on dry running surfaces. The static friction coefficient is m_μ = 0,55 and the running speed is 71,2241 km/h, conformed as shown in Figure 19. The values of the wheelset drive system parameters are the basic ones. The track is provided with elastic rail pads.

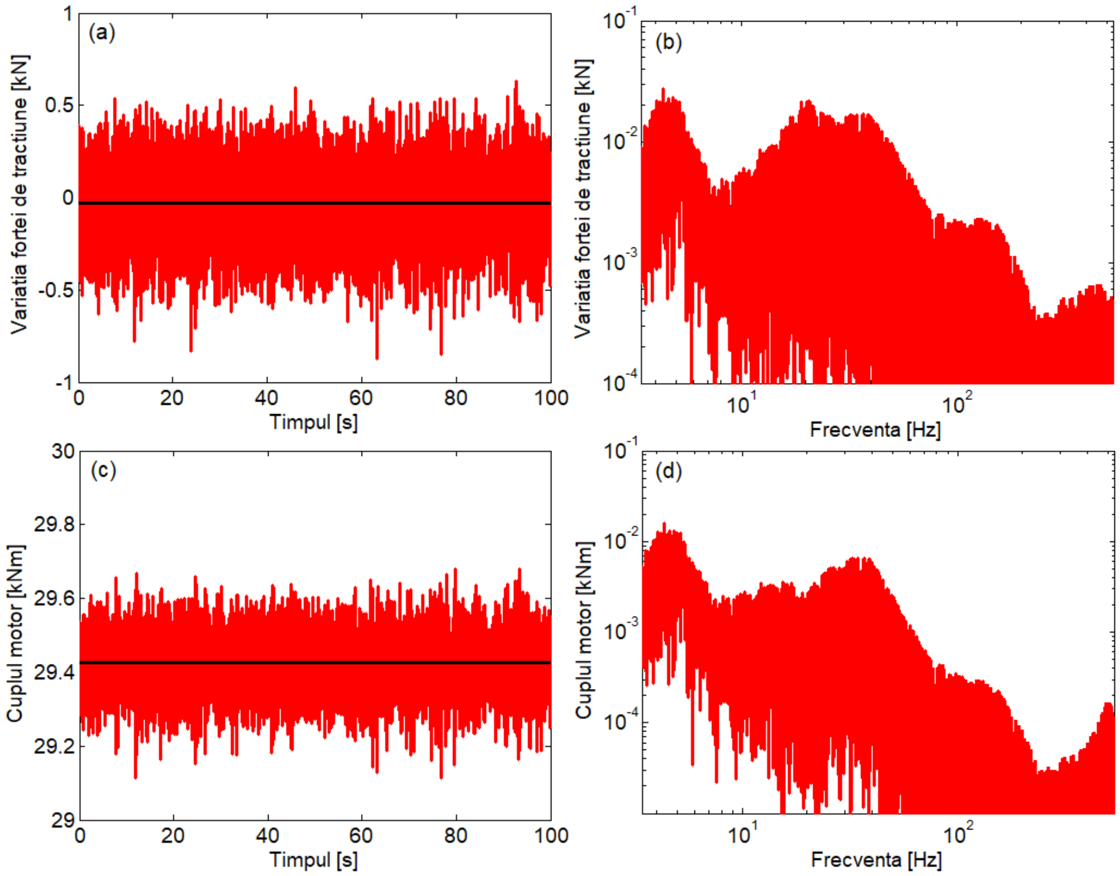

Fig. 39 Variation of the tractive force and motor torque when driving on a track with elastic rail pads, dry running surfaces, m_μ = 0,55, V = 71,2241 km/h (damping degrees: 0,1): (a) variation of the tractive force; (b) the amplitude spectrum of the change in the tractive force; (c) the motor torque at the wheelset; (d) the amplitude spectrum of the motor torque at the wheelset.

Characteristic of the stationary regimes located on the stable branch of the friction force curve is the fact that the variation of the frictional force has only a positive damping effect, which contributes to the attenuation of the vibration regime of the wheelset. Thus, the effective values of the variation of traction force and wheelset motor torque reach only 0.177 kN and 0.073 kNm respectively. Comparing these values with those obtained under similar traffic conditions, but at the stationary regime located on the unstable branch of the friction force curve, there is a decrease of more than 8 times in the variation of the traction force and a reduction of more than 5 times in the variation of the motor torque.

Due to the increase in depreciation due to the positioning of the stationary regime on the stable branch of the friction force curve, the amplitude spectra (diagrams (b) and (d) of Figure 39) change significantly, showing different shapes in relation to those obtained previously (see Fig. 36 diagrams (b) and (d)).

On the one hand, the amplitudes of the spectral components are greatly reduced compared to the previous situation when the stationary regime was positioned on the unstable branch of the friction force curve. On the other hand, there is a change in the 'hierarchy' of amplitude resonances in the sense of diminishing the importance of the amplitude resonance of the wheelset recoil and increasing as a share of the amplitude resonance due to the salting of the suspended mass of the bogie and the resonance of the rigid mode of vertical vibration of the wheelset by the way.

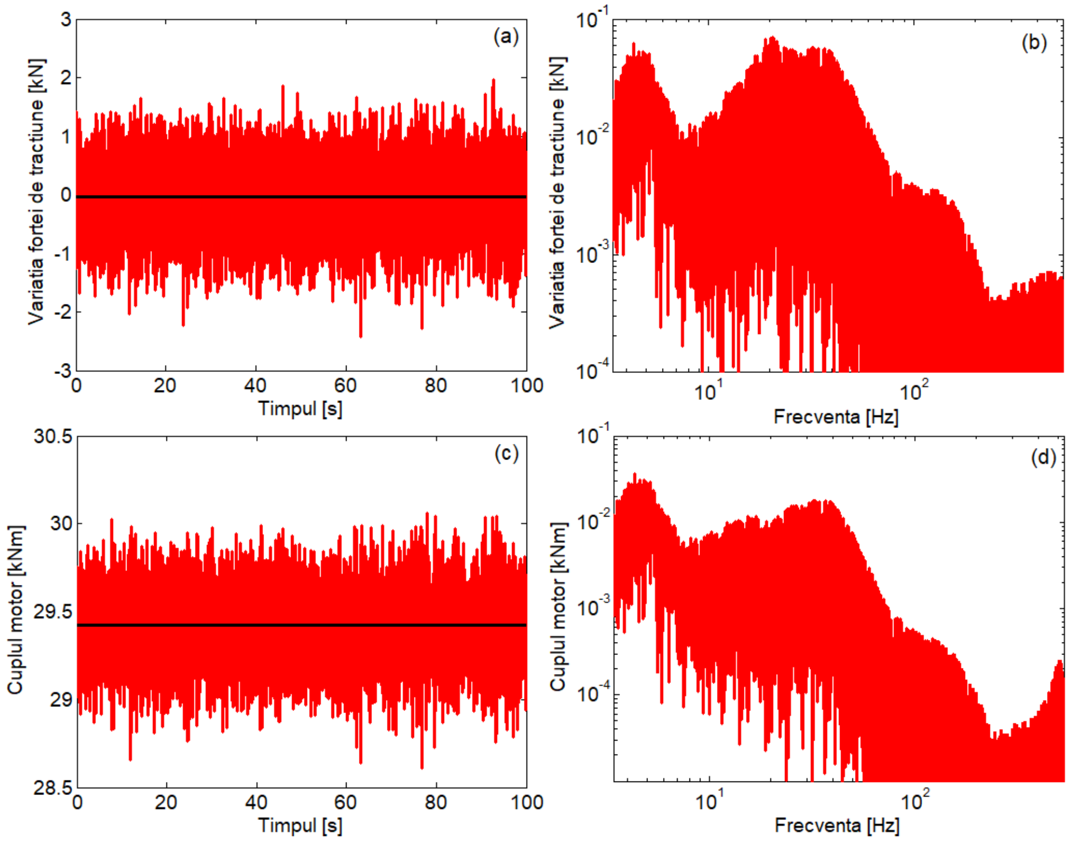

Fig. 40. Variation of traction force and motor torque when driving on a track with elastic rail plates, wet running surfaces, m_μ = 0,55, V = 70,7122 km/h (damping degrees: 0,1): (a) variation of traction force; (b) the amplitude spectrum of the change in the tractive force; (c) the motor torque at the wheelset; (d) the amplitude spectrum of the motor torque at the wheelset.

If the treads are wet, then the positive damping effect of the variation of the frictional forces induces is lower as the slope of the friction force curve as a function of the sliding speed is lower as seen in Figure 15. As a result, the regime of the longitudinal vibrations of the driving wheelset is more intense as can be seen in Figure 40 showing the variation of the traction force and the motor torque at the wheelset when running on wet running surfaces (m_{μ} = 0,55). The running speed is 70.7122 km/h and ensures the achievement of the nominal torque of the motor, 29,443 kNm. The effective value of the traction force variation is 0,515 kN and the effective value of the motor torque is 0,186 kNm, values much higher than those obtained in the case of dry running surfaces under the same conditions (m_{μ} = 0,55 and the motor torque = nominal torque): 2,9 times higher for the variation of the traction force and 2,5 times higher for the effective value of the motor torque at the wheelset.

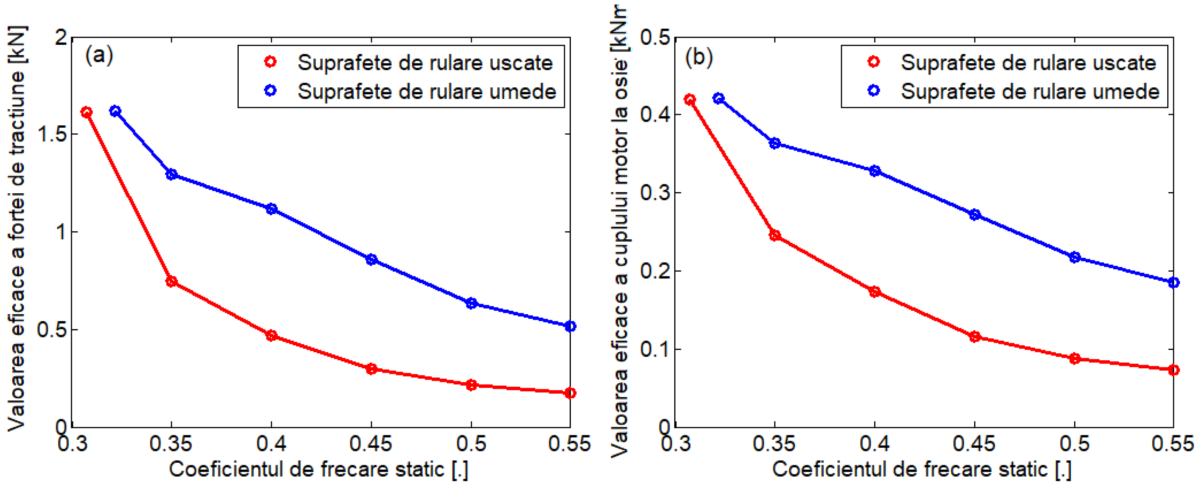

Fig. 41. Effective values of the tractive force and wheelset motor torque variation:

The way in which the condition of the treads influences the longitudinal vibration regime at the adhesion limit is shown in Figure 41. The conditions allowing the development of the nominal motor torque for dry and wet treads were considered to be the conditions that allow the development of the rated motor torque. It is noted that as the coefficient of static friction decreases and the driving wheelset reaches the adhesion limit, the effective values describing the intensity of the vibration regime increase greatly, more than 3 times in the case of traction force variation on wet surfaces and 9 times in the case of dry running surfaces. Effective motor torque values increase by more than 2 times when running on wet surfaces and almost 6 times for dry treads.

It is interesting that at the limit of adhesion, the condition of the treads does not influence the intensity of the longitudinal vibration regime. The explanation lies in the fact that regardless of the condition of the treads (dry/wet), the effect of the frictional force variation is the same as the slope to the frictional force curve is zero.

6. Experimental determinations

In this chapter are presented three experimental determinations, two being made on stands from the Department of Railway Vehicles of the Faculty of Transport, POLITEHNICA University of Bucharest, and the third determination was made with an electric locomotive LE 5100 kW. These determinations are designed to validate the models used in this thesis.

A first set of tests were aimed at validating the model for the study of torsion vibrations of the wheelset. For this, the unitary efforts in the body of an wheelset model subjected to torsion deformation due to priming the phenomenon of stick slip were determined. On this basis, the natural torsion frequency of the wheelset model was determined and this was compared with the theoretical result obtained by applying the model elaborated in chapter 3 to the characteristics of the wheelset model.

The second set of tests concerned the validation of the model of the mechanical characteristic of a three-phase asynchronous electric motor. A stand for determining the mechanical characteristic of a three-phase electric motor was designed and elaborated by the author of the work. The experimental results were compared with the theoretical results obtained using the motor torque calculation relationship taking into account the values of the parameters of the experimental motor.

The third set of tests was carried out on the running of an electric locomotive while towing a freight train and consisted of measuring accelerations at the level of the locomotive's wheelset boxes. The purpose of these tests is to validate the model of vertical interaction between the driving wheelset and the track.

6.1. Determination of torsion vibrations of the driving wheelset

The experimental determinations for the validation of the model for the study of torsion vibrations of a driven wheelset were made on a stand located in the Laboratory of Dynamics and Structures of the Department of Railway Vechicles of the Faculty of Transport, Politehnica University of Bucharest, the stand being illustrated in Figure 41.

Fig. 42. Experimental stand for the determination of the torsion of the driving wheelset

The stand consists of a driven wheelset driven by a longitudinally arranged three-phase asynchronous motor, the motor torque being transmitted to the wheelset by a tapered gear with straight teeth and a drive shaft connecting the motor to the gear. The drive speed of the wheelset can be varied in two stages by changing the connection of the motor phases (star-triangle connection). The loading of the wheelset is carried out by means of two mobile rails provided with friction elements that are put in contact with the surface of the wheels. The contact force shall be modified by a hand-operated screw tightening system. The rail contact force on the two wheels shall be measured by a tensometric guage. The measurement of the torsion moment in the driving wheelset is carried out by a full bridge consisting of four strain guage arranged in directions that make an angle of 45 degrees with the median axis of the wheelset.

The excitation and actual measurement of the bridge is made by module NI 9219 designed for voltage and current measurements in applications of resistive electrical tensometry, temperature measurements by means of thermocouple transducers and electrical resistance measurements. The module is connected to the computer via the NI cDAQ 9174 chassis. Equipment control, recording and further processing of the results is carried out with a program developed in Matlab.

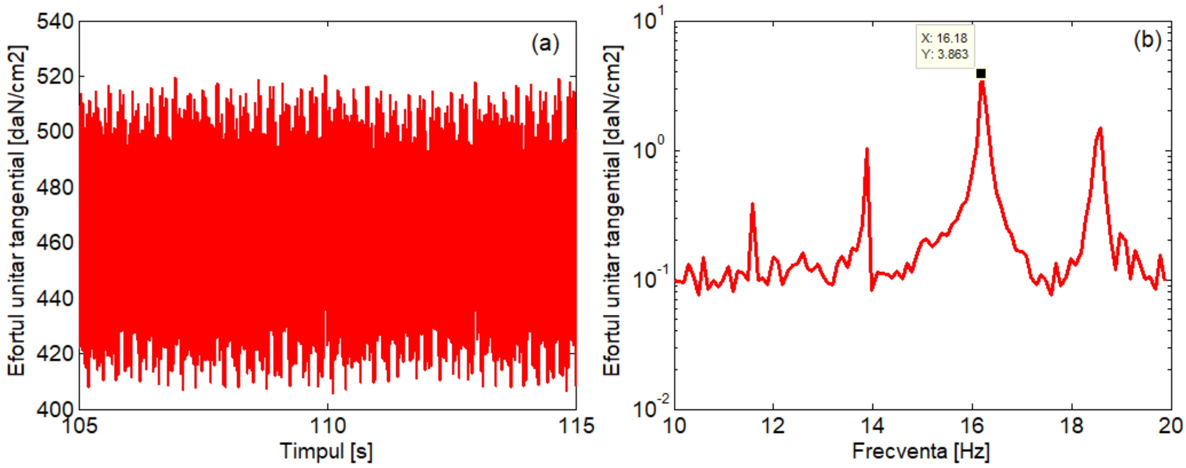

Fig. 43. Tangential unit effort in the scale wheelset: (a) variation over time; (b) the amplitude spectrum.

With the stand and the measurement system shown above, determinations were made for several values of the load of the driving wheelset layout and the output voltage from the measuring device was recorded. This is proportional to the specific deformation which in turn is proportional to the tangential unit effort from the recording of which a sequence is shown in Figure 43 (a).

It is noted that the vibration has a relatively regular appearance characteristic of a boundary cycle. In order to find out the most important component of this limit cycle, Fourier analysis can be applied for the purpose of constructing the amplitude spectrum (see fig. 43 (b)). The amplitude spectrum of the tangential unit efforts has the most important spectral component at the frequency of 16,18 Hz.

In order to validate the model and the simulation program presented in chapter 3 of the work, it is necessary to perform the numerical simulation using this time the geometric and inertial parameters of the wheelset model and compare the results obtained numerically with those obtained experimentally.

The torsion receptance of the wheelset is shown in Figure 44, from which it is noted that the resonance frequency obtained is 16,8 Hz. This value is close to the experimentally determined frequency value (16,18 Hz).

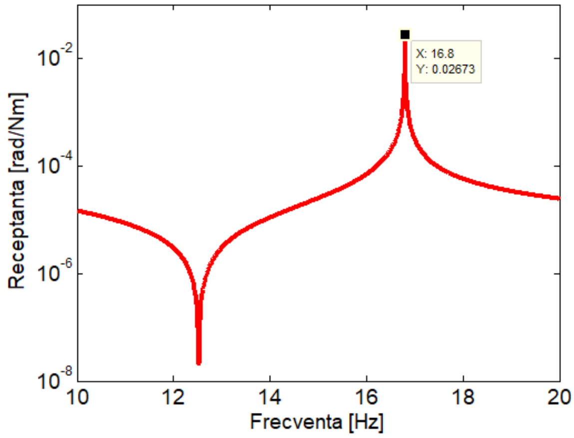

Fig. 44. Receptance of the driving wheelset obtained by numerical means

The difference stems from measurement errors taking into account that the geometric parameters of the stand wheelset were measured with a certain degree of approximation, and the inertial parameters were determined using the Ansys program by approximate three-dimensional modeling of the wheelset. In percentage terms, the difference between theoretical and experimental results is 3,7 % which allows the validation of the model developed for the study of torsion vibrations of the driving wheelset.

6.2. Determination of the mechanical characteristic of the three-phase asynchronous motor

To determine the mechanical characteristic of the three-phase asynchronous motor, a stand consisting of a three-phase asynchronous motor with 4 poles, whose mechanical characteristic is intended to be determined, drives a DC machine that works in dc current generator mode for charging the studied motor (fig. 45).

Fig. 45. Stand asynchronous machine – DC machine.

For the operation and adjustment of the asynchronous machine, a static frequency converter is used, and the adjustment of the generator is carried out by varying the excitation current from a variable current source.

Fig. 46. Measuring instruments used to determine the electrical operating parameters of electric machines.

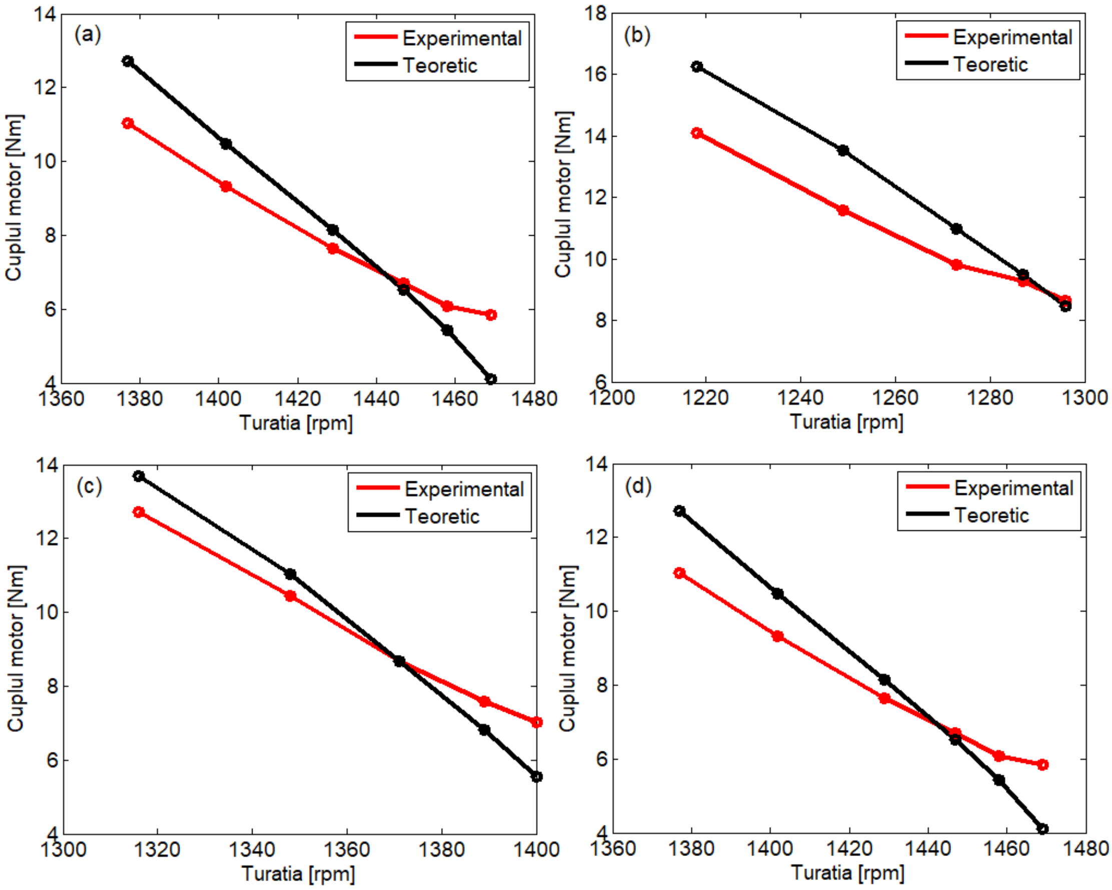

Fig. 47 Comparison of experimental and theoretical motor torque results according to the frequency of the supply voltage: (a) at 25 Hz; (b) at 45 Hz; (c) at 48 Hz; (d) at 50 Hz.

The measurement of operating parameters is carried out as follows: the measurement of stabilized electrical parameters using multimeters, the speed is measured by means of a non-contact digital tachometer, the temperature is measured with an infrared thermometer, and the power factor is measured with a power factor meter. At the same time, the voltage and the line current are recorded with an oscilloscope. The measuring instruments used are illustrated in Figure 46.

Figure 47 shows, for example, a part of the results obtained experimentally in determining the torque of the three-phase asynchronous motor asynchronous as a function of the speed at several frequencies of the supply voltage. The corresponding curves calculated using the theoretical model are also presented.

Analyzing the results obtained, a satisfactory concordance can be observed: all the results have the same trend and the values are relatively close. The differences between calculated torque and determined torque are due to measurement errors - all instruments used to measure electrical parameters have a degree of error of up to 3%. Moreover, the torque actually developed by the electric motor was not determined directly, but indirectly on the basis of the calculation of the electric power absorbed by the motor from the frequency converter and on the basis of the efficiency curve of the motor (starting from the nominal value of the efficiency and the universal characteristic of the efficiency of a three-phase asynchronous motor of low power).

In conclusion, based on the above, the theoretical model of the three-phase asynchronous motor is validated by the results obtained experimentally.

6.3. Measurement of vertical accelerations of driving wheelsets in electric locomotive LE 5100 kW

The following are the results of the measurement of vertical accelerations at the level of the wheelset boxes of an electric locomotive LE 5100 kW, a determination made under real operating conditions, the locomotive being on the way and performing the service of towing a freight train.

Fig. 48 Accelerometer located on the box of wheelset 4 of the locomotive.

Fig. 49. Accelerometer located on the box of wheelset 6 of the locomotive.

The purpose of these experimental determinations is to validate the model of vertical interaction between the driving wheelset and the running track, as set out in Chapter 4.

The equipment used for acceleration measurements is that presented in the experimental determination of the torsion vibrations of the driving wheelset, with the difference that the NI module used this time is specific to the measurement of piezoelectric accelerometers, and the effective measurement of accelerations was carried out using piezoelectric accelerometers.

In order to carry out the measurements, accelerometres were fitted to wheelsets 4 and 6 of the locomotive as can be seen in figures 48 and 49.

Fig. 50. Overview from the cab of station 2 driving

The accelerometer signals are taken over by the National Instruments purchasing system (ni cDAQ 9174 chassis and ni 9234 modules attached), which is located inside the locomotive. The control and recording of data is carried out using a laptop located in driving post II of the locomotive (non-active post during the movement – see fig. 50).

The recording of the speed at which the locomotive travels was done using a mobile terminal running the Android operating system and the BasicAirData GPS Logger application (application available free of charge in the Play Store), the data being used to correlate the records of the accelerometers with the speed of movement of the locomotive, correlation made after the recording.

The route traveled by the locomotive during the determinations sums up a distance of 157 kilometers and starts from Teleajen – Ploieşti to Roşiorii Nord area, via Ploieşti Sud, Ploieşti Triaj, Chitila, Chiajna, Grădinari, Videle. The route taken is shown in Figure 34. The maximum speed of travel was 70 km/h.

Several measurements of accelerations at different speeds of traffic were carried out on different sections of the mentiones route.

For example, Figure 51 shows the accelerations measured at the wheelset boxes and on the bogie frame near wheelsets 4 and 6 during traffic at a speed of 66 km/h, a value close to that taken into account in this work.

It is noted that the acceleration at the level of the bogie frame is noticedly lower than that at the level of the wheelset boxes, which can be explained by the filtering effect due to the primary suspension. Indeed, the effective acceleration values are as follows: 2,02 m/s^2 at wheelset 4, 1,48 m/s^2 at wheelset 6 and 0,38 respectively on the bogie frame above wheelset 4 and 0,21 m/s^2 at wheelset 6.

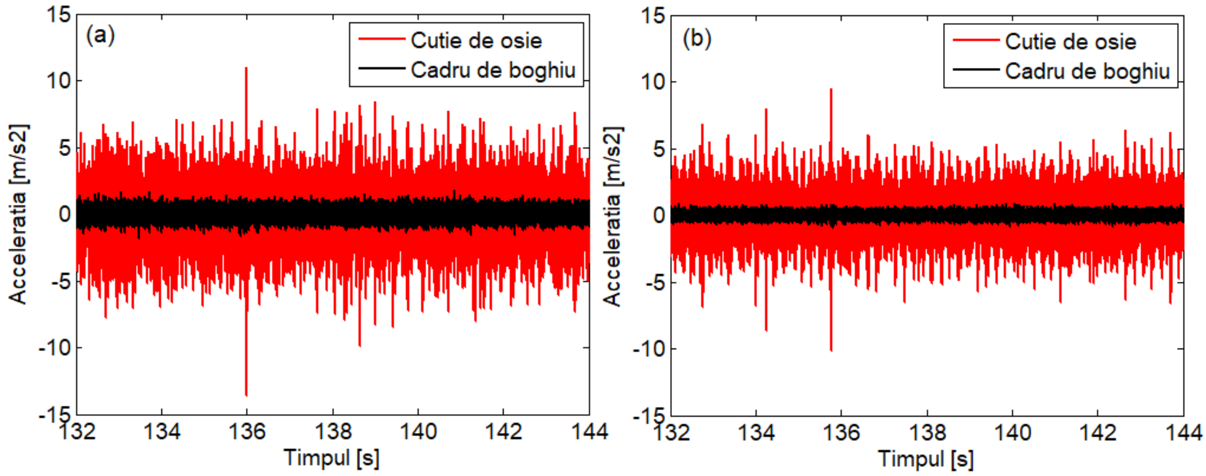

Fig. 51 Acceleration measured at a speed of 66 km/h: (a) at wheelset 4; (b) at wheelset 6.

For the study presented in this paper, the highest interest is the acceleration of the wheels that was measured at the level of the wheelset boxes. As the theoretical model takes into account a single driving wheelset, the comparison between theoretical and experimental results will concern the average of the accelerations measured at the level of the two wheelsets.

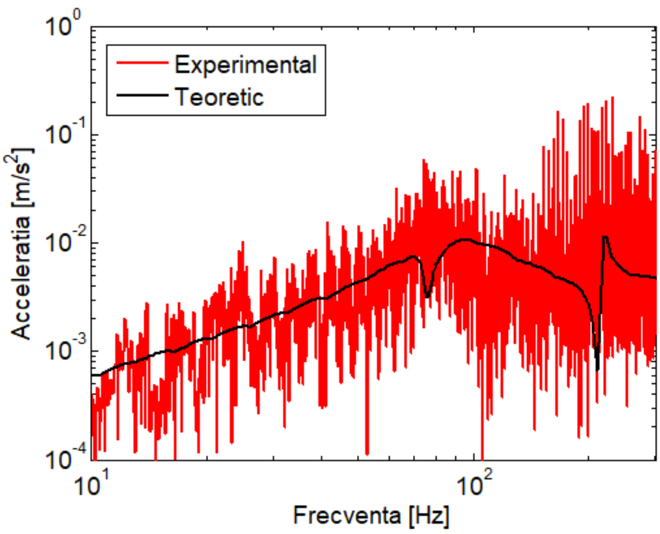

Fig. 52. Illustrative for the comparison between the measured and calculated wheel accelerations.

Figure 52 shows the average throttle spectrum measured at the two wheelsets and the throttle spectrum obtained using the vertical interaction model between the driving wheelset and the running track shown in Chapter 4. The theoretical results were obtained from the calibration of the model parameters and excitation by the frequency analysis method.

It is noted that there is a qualitative concordance between theoretical and measured results. In assessing that comparison, it must be taken into account that there are no experimental data on the properties of the track or on the level of irregularities in running surfaces.

In conclusion, it can be appreciated that the theoretical model presented in this paper satisfactorily describes the phenomena of the vertical interaction between the driving wheelset and the track.

7. Conclusions, original contributions, and future directions of research

The driving wheelset of electric traction railway vehicles are exposed to vertical vibrations caused by interaction with the running track in the presence of surface irregularities, vibrations which are liable to parametrically excite the longitudinal vibrations of the drive system of the driving wheelset and their elastic driving system.

Taking into account the influence of vertical vibrations on the behavior of the driving wheelset gives a clearer picture of what happens when the traction vehicle is travelling on the track.

The effects of these vibrations have an impact on the traction performance, especially when the vehicle is travelling at rated speed, the electric motor is operating at rated power and the friction between the wheels and the rails is at the limit of adhesion. This is the most important operating mode of a traction unit according to the traction limit characteristic.

The study of the vibrations of the drive system of the driving wheelset and its driving system at the nominal mode of the traction limit characteristic shall highlight how the main design and functional parameters can influence the traction performance of the driving wheelset and allows, on this basis, to identify the possibilities for improving these performances.

The doctoral thesis 'The study of the wheelset - track interaction in the railway traction vehicles' proposes a flexible and comprehensive model at the same time for the investigation of the phenomena specific to the real-life circulation of the driving wheelset at the nominal regime of the traction limit characteristic and makes important contributions through the better knowledge of the ways of improving the running apparatus of the traction vehicles.

7.1. Conclusions

In constant-speed running on an straight leveled track, the longitudinal vibrations of a driving wheelset driven by an electric motor operating at standstill may be excited by variations in motor torque caused by the upper harmonics of the electro-magnetic field or by the variation of vertical contact forces between the wheels and the rails as a result of interaction with the track. Considering only the second excitation mechanism, it follows that the study of the interaction between the driving wheelset and the running track requires to be taken into consideration the bending and torsion vibrations of the driving wheelset.

The interaction between the driving wheelset and the running track is conditioned by the mechanical properties of the two subsystems that determine their frequency response.

Conclusions on the dynamic response of the driving wheelset.

The driving wheelset equipping the railway traction vehicles are, as a rule, fitted with unilateral transmission and are driven by asynchronous short-circuit rotor electric motors. The unilateral transmission determines the asymmetry inertia of the driving wheelset both in terms of bending and torsion vibrations.

The bending receptances of the driving wheelset is different next to the two wheels both in the case of symmetrical excitation and in the case of antisymmetric excitation, the bending receptation being lower to the wheel near which the geared crown is mounted due to its contribution.

The torsion receptance of the driving wheelset to the wheel next to the geared crown is less than the receptance of the other wheel at frequencies lower than that of the first elastic torsion mode and higher, otherwise.

By wearing out the wheels, the natural frequencies of the elastic vibration modes increase, and the receptance next to the wheels are reduced because the wheelset inertia, regardless of the type of vibration, is lower in the case of semi-exposed or worn wheels.

The vibration modes of the driving wheelset are symmetrical and antisymmetric, and due to the inertial asymmetry of the wheelset, the two types of vibration modes are coupled with each other.

Changing the position of the toothed crown has the effect of altering the resonant frequencies of the driving wheelset. If the crown is in the middle, between the wheels, the structure of the driving wheelset becomes symmetrical, and the symmetrical modes are decoupled from the antisymmetric ones.

The bouncing and pitch vibrations of the bogie's suspended mass of the driving wheelset are coupled with the rigid wheelset modes (bouncing and pitch) and cause the natural frequencies of the wheelset elastic bending modes to be reduced due to the inertia introduced by the suspended mass of the bogie. The damping of the primary suspension reduces the wheelset response both to its own bouncing and pitch frequencies resulting from the coupling of the suspended mass with the driving wheelset, and to the frequency of the first elastic bending mode. It is therefore recommended that, in general, the study model of the wheelset-track interaction should include the effect of the bogie's suspended mass and primary suspension.

Conclusions on the dynamic response of the track

The frequency response of the track expressed by the receptation of the rail in the range of 0 -6-700 Hz has two resonant frequencies, one low, at which the rail and sleepers vibrate in phase, and the other high, where the rail and sleepers vibrate in antiphase. Between the two resonant frequencies, there is an anti-resonance frequency due to the dynamic absorbing effect of the sleepers in relation to the rail. At frequencies greater than 6-700 Hz, the receptation of the rail is influenced by the distance between the sleepers.

Rail pads play a very important role in the dynamic response of the track through their rigidity and damping characteristics. In current practice, elastic or rigid rail pads are used, made of rubber or other materials with viscous-elastic properties.

The use of rigid rail pads leads to the hardening of the track which translates into the reduction of the track receptation to low and medium frequencies. In addition, it increases the anti-resonance frequency and the high resonance frequency of the track, which makes that in the frequency range taken into account, the receptation of the rail is higher compared to the situation in which the rail pads are elastic.

The dynamic response of the rail depends on the damping of the track components respectively on the damping introduced by the rail plates and the ballast bed. However, the results of the numerical simulations show the importance that the type of damping model has in terms of the theoretical value of the track receptation. The most common damping models are the proportional damping model and the hysterical damping model. The first model can be used for both frequency analysis and time analysis, but the results have a limited scope of accuracy as dissipated energy increases in proportion to frequency, which contradicts experiments that show a limited frequency dependency. The results obtained with the help of hysteretic damping are closer to the experimental ones, but this model, being a purely mathematical model in the sense that it describes the phase shift between force and displacement in the harmonic case, can only be applied in the frequency field.

The parallel use of the two damping models shows that amplitude resonances occur at slightly different frequencies from one model to another, but the amplitude of the receptance changes significantly, which leads to the distortion of the frequency response.

Conclusions on the vertical interaction of drive wheelset – track

The system consisting of the suspended mass of the bogie, the driving wheelset, the elastic contact between the wheels and the track has the following resonances: two resonances due to the bouncing and pitch movements of the suspended mass on the primary suspension, two resonances corresponding to the vibration of the wheelset as a rigid body on the track (bouncing - pitch) and three resonances between the rail anti-resonance frequency and the high resonance frequency, corresponding to the elastic bending modes of the wheelset on the track.

The frequency response functions of the elements of interest, the displacements of the wheels and rails in the contact sections, as well as the vertical contact forces, are different from one wheel to another due to the asymmetry of the driving wheelset. Damping turns resonances into amplitude resonances, and if the resonant frequencies are close, then the peaks of the amplitude resonances are merged (e.g. bouncing and pitch of the suspended mass on the primary suspension or bouncing and pitch of the wheelset on the track).

The effect of roughness on the vertical vibration regime of the driving wheelset and track has been studied in correlation with the rigidity of the rail pads and the wear state of the wheels.

For the theme of this work, the most important interest is the vertical contact force, and that is why it is further referred only to it.

The amplitude spectrum of the vertical contact force shows local highs and lows as follows. The local maximums of the vertical contact force correspond to the bouncing and pitch of the suspended mass of the bogie on the primary suspension, to the rigid modes of vibration of the wheelset on the track and to the anti-resonance regime of the rail, the frequency of the last being influenced by the rigidity of the rail plates. The local minimums of the vertical contact force are next to the resonant frequencies of the bouncing - pitch movements of the suspended mass that are coupled with those of the driving wheelset and the low and high resonance frequencies of the rail.

In the range of low frequencies, lower than the resonant frequency of the rigid modes of vibration of the wheelset on the track, the vertical contact force is greater if elastic rail plates are mounted in the track. At higher frequencies, however, the situation is reversed in the sense that the vertical contact force is lower in the case of elastic rail plates.

The wear condition of the wheels of the driving wheelset has less influence on the vertical contact forces. It may be noted, however, that at frequencies below the resonant frequency of the rigid modes of vibration of the wheelset on the track, running with new wheels is accompanied by relatively higher vertical contact forces.

Conclusions on the longitudinal vibrations of the drive system of the driving wheelset and the driving system

Given the adhesion conditions (static friction coefficient and the condition of the running surfaces), and given the fact that the slippage of the motor depends on the creepage of the wheels on the rails, it follows that, at a certain speed of traveling, the stationary regime is set at that value of the creepage at which the balance between the motor torque at the wheelset and the torque of the frictional forces is obtained.

The analysis of the stationary regime of the driving wheelset at rated speed according to the traction characteristic shows that it is not possible to achieve the nominal value of the motor torque due to the effect of the creepage of the wheels on the rails on the motor slip. The motor torque actually developed depends on the condition of the treads in the sense that if the treads are dry then the actual torque is higher than if the surfaces are wet. However, in order for the motor to develop the rated torque, the running speed needs to be reduced in relation to the nominal value, and this reduction becomes significant if the running surfaces are wet.

It has been shown that for a given stationary regime, the efficiency of the driving wheelset depends solely on the creepage corresponding to that stationary regime in that the reduction in efficiency is equal to the increase in creepage. As the amplitude of the creepage depends on the condition of the treads, being larger if the treads are wet, it follows that for these conditions the efficiency of the driving wheelset is affected. At the same time, the yield decreases as the grip conditions worsen, and the wheelset approaches the grip limit. As a result, it is recommended to avoid circulation at the limit of adhesion, especially in conditions where the treads are wet, because it decreases the efficiency of traction. The existence of the locomotive's anti-slip system avoids exceeding the adhesion limit and the appearance of stick slip vibrations, but it cannot reduce the pseudo-slipness of the driving wheelset for this one depends solely on the force of adhesion and the condition of the running surfaces.

Linear stability analysis shows that, reflecting the damping of the elastic coupling between the torsion shaft and the reducing gear, as well as the damping of the wheelset guiding system, at the adhesion limit, the driving wheelset is at the limit of stability, regardless of whether the treads are dry or wet; the regime at the adhesion limit is simply stable. Under the same conditions, the stationary regimes on the ascending (stable) branch of the friction force curve as a function of the sliding rate are asymptotically stable, and those on the descending (unstable) branch are unstable. The stable/unstable nature of the stationary regimes shall be explained by the contribution of the dynamic component of the frictional force which may introduce positive or negative damping depending on the branch on which the stationary regime is located.

The analysis of the nonlinear stability of the unstable stationary regimes (located on the unstable branch) showed that, in the absence of any depreciation, two stable limit cycles called torsion and rebound limit cycles are possible.

The limit cycle of torsion is the frequency close to the resonance frequency of the first elastic torsion mode of the driving wheelset. It is characterized by being accompanied by significant armonic components of motor torque and the torque of frictional forces that can affect the mechanical strength of the wheelset.

The rebound limit cycle develops practically at the resonance frequency of the rebaund movement of the wheelset connected by the elastic conduction system to the bogie frame and is manifested by very large oscillations of the traction force.

The exity of limit cycles is justified by the fact that an energy balance is reached between the accumulated energy and that dissipated during a period of the dynamic component of the frictional force which has a negative or positive dampening effect depending on the branch of the friction force curve on which it works.

The damping of the elastic coupling or that of the wheelset steering system limits the areas in which the limit cycles may exist. Moreover, if the wheelset drive system and the driving system are properly damped, then the unstable stationary regime becomes asymptotically stable. As a result, traction performance can be improved when the wheelset is travelling at the adhesion limit by providing the necessary damping in the drive and guiding systems.

The analysis of longitudinal vibrations maintained by variations in frictional forces induced by variations in vertical contact forces leads to the following conclusions.

If the driving wheelset runs at the adhesion limit, then the variations in traction force and motor torque are almost insensitive to the type of rail pads (elastic/rigid) with which the track is fitted.

The variation in traction force is strongly influenced by the relative positioning of the wheelset's own rebaund frequency in relation to the resonant frequency of the rigid modes of vibration of the wheelset on the track, in the sense that the effective value of the traction force can also increase by 2-3 times if the two frequencies are close together.

As a result, it is recommended that when designing the elastic guiding system of the driving wheelset, a calculation be carried out to check the positioning of the resonant frequencies.

If the running parameters of the driving wheelset correspond to the stationary regime on the stable branch of the friction force curve as a function of the sliding speed, the dynamic regime improves substantially due to the effect of positive damping.

Running on wet treads is clearly unfavourable compared to running on dry treads due to the fact that the positive damping effect is weaker, the slope of the friction force curve depending on the sliding speed is noticeably lower.

However, at the adhesion limit, the condition of the treads does not influence the intensity of the longitudinal vibration regime, since regardless of the fact that the treads are dry or wet, the effect of the frictional force variation is the same since the slope to the friction force curve is zero.

For the validation of the models used in this work, a consistent program of experimental tests focused on three directions of interest was developed: the torsional vibrations of the driving wheelset, the mechanical characteristic of the asynchronous motor and the vertical vibrations of the wheelset.

The comparison between the experimental and theoretical results allowed the validation of the following models: the model for the study of torsional vibrations of the driving wheelset, the model of the mechanical characteristic of the asynchronous motor and the model of vertical interaction between the driving wheelset and the running track.

7. 2. Original contributions

In relation to the results of the analysis of the current state of research in the field of the thesis, respectively the interaction between the driving wheelset and the track under nominal traffic conditions according to the traction characteristic, the following are presented as the most important personal contributions.

- drawing up the mechanical model for the interaction between the driving wheelset and the running track comprising the following original aspects: (a) the structure of the model including the vertical vibration model of the driven wheelset and the track and the longitudinal vibrations model comprising the motor drive system of the driving wheelset and its driving system; (b) the parametric excitation mechanism induced by the variation of the frictional forces due to the variation of the vertical contact forces which makes it possible to assess the traction performance of the driving wheelset under traffic conditions close to the actual ones; (c) the application of the hysteretic damping model to improve the amplitude and phase spectra of the variation of vertical contact forces and their transformation into a pseudo-time function representing the parametric excitation factor of the longitudinal vibrations of the driving wheelset and the use as such in the integration of equations of motion;

- elaboration of mathematical models which consisted in inferring the equations of motion associated with mechanical models by applying the principles of classical mechanics;
- elaboration of numerical models derived from mathematical models that allowed to perform numerical applications of the thesis;
- analysis of the frequency response of a one-sided driving wheelset for torsion and bending vibrations and highlighting the influence of inertia asymmetry and the state of wear of the wheels on the receptances calculated next to the wheels;
- analysis of the vertical vibrations of the driving wheelset when running on the track in the presence of irregularities of the treads in correlation with the damping model of the track, the inertial asymmetry of the driving wheelset and the state of wear of the wheels;
- elaboration of a method for obtaining the amplitude spectrum of tread irregularities starting from the roughness level spectrum;
- analysis of the stationary regime of the wheelset drive system when the motor develops the rated torque, depending on the friction coefficient of wheels and rails taking into account the condition of the running surfaces; the electric motor may develop the rated torque only if the speed is reduced in relation to the nominal speed of the traction characteristic when slipping to compensate for the effect of the creep of the wheels on the slippage of the motor;
- calculation of the mechanical efficiency of the driving wheelset according to the coefficient of friction between the wheels and the rails in correlation with the condition of the running surfaces; the mechanical efficiency of the driving wheelset causes significant decreases in the case of wet surfaces and/or when travelling at the adhesion limit;
- analysis of the linear stability of the stationary regime of the drive system of the driving wheelset corresponding to the rated operating regime of the electric motor according to the traction characteristic of the locomotive and according to the variation of the coefficient of friction between the wheels and the rails;
- analysis of the nonlinear stability of the unstable stationary regimes and highlighting the existence of two stable limit cycles, one of torsion of small amplitudes and the frequency close to the resonance frequency of the first elastic mode of torsion of the driving wheelset, and the other, of rebound with higher amplitudes at the resonant frequency of the rebound movement of the wheelset connected by the elastic driving system to the bogie frame;
- determining the influence of the damping of the elastic coupling between the wheelset and the driving system on the existence of the limit cycles by means of the Hopf bifurcation diagram and demonstrating the possibility of eliminating the instability of the stationary regimes located on the unstable branch of the friction force curve as a function of the sliding speed by ensuring proper damping of the elastic coupling and the elastic wheelset driving system;

- analysis of the longitudinal vibration regime of the drive system of the driving wheelset and of the driving system maintained by the variations in the vertical contact force as a result of the interaction between the wheelset and the track in the presence of tread irregularities; changes in motor torque and tractive force have been shown to depend on the condition of the treads (dry/wet) unless the wheelset is travelling at the adhesion limit;
- experimental validation of the mechanical model of the driving wheelset for the study of torsion vibrations using a didactic and research stand;
- the design and construction of an experimental stand for the determination of the mechanical characteristic of the three-phase asynchronous AC machine and the validation by experiments of the theoretical mechanical characteristic used in the work to simulate the motor torque developed by the asynchronous motor; the built stand allows carrying out didactic and research activities;
- experimentally validating the model for the vertical interaction of the driving wheelset with the track based on the acceleration measurements at wheelset box level made with an electric locomotive (LE 5100 kW) in the current-line traction service of a freight train.

7. 3. Future research directions

The research topic can be developed according to the following directions of research:

- the starting mode of the traction unit, in particular when the start-up takes place at the adhesion limit;
- influence of motor torque harmonics induced by the control system of the asynchronous motor (the static converter);
- running on connection and circular curves.

Selected bibliography

1 Aster, R. C., Borchers, B., Thurber, C. H., *Parameter estimation and inverse problems*, Elsevier, 2018.

2 Ayasse, J. B., Chollet, H., Wheel-rail contact. *Handbook of railway vehicle dynamics*, 85-120, 2006

3 Baeza, L., Vila, P., Xie, G., Iwnicki, S. D., *Prediction of rail corrugation using a rotating flexible wheelset coupled with a flexible track model and a non-Hertzian/non-steady contact model*, Journal of Sound and Vibration, 330(18-19), 4493-4507, 2011.

4 Bosso, N., Zampieri, N., *Experimental and numerical simulation of wheel-rail adhesion and wear using a scaled roller rig and a real-time contact code*, Shock and Vibration, 2014.

5 Chen, H., Ishida, M., Namura, A., Baek, K. S., Nakahara, T., Leban, B., Pau, M., *Estimation of wheel/rail adhesion coefficient under wet condition with measured boundary friction coefficient and real contact area*, Wear, 271(1-2), 32-39, 2011.

6 De Pancorbo, S. M., Ugalde, G., Poza, J.,Egea, A., *Comparative study between induction motor and synchronous reluctance motor for electrical railway traction applications*, 5th international electric drives production conference (EDPC) (pp. 1-5). IEEE, 2015.

7 Doi, H., Miyamoto, T., Nishiyama, Y., Ohe, S., Kamachi, H., *A new experimental device to investigate creep forces between wheel and rail*, Wear, 271(1-2), 40-46, 2011

8 Dumitriu, M., **Gheți, M.A.**, *Evaluation of the vertical vibrations behaviour of the bogie at failure of the dampers in the primary suspension of the railway vehicle*, MATEC Web of Conferences - Vol. 178, 2018, Numărul articolului 06001.

9 Dumitriu, M., **Gheți, M.A.**, *Cross-correlation analysis of the vertical accelerations of railway vehicle bogie*, Engineering, Procedia Manufacturing, Vol. 32, 2019, pp. 114-120.

10 Dumitriu, M., **Gheți, M.A.**, Cruceanu, I.C., *Experimental analysis of the vertical vibration of the railway bogie during braking*, Procedia Manufacturing, Vol. 46, 2020, pp. 49-54.

11 Dumitriu, M., **Gheți, M.A.**, *Influence of the interference of bounce and pitch vibrations upon the dynamic behaviour in the bogie of a railway vehicle*, IOP Conference Series: Materials Science and Engineering, 2018, Vol. 400.

12 Dumitriu, M., **Gheți, M.A.**, *Numerical study on the influence of primary suspension damping upon the dynamic behaviour of railway vehicles*, IOP Conf. Series: Materials Science and Engineering, Vol. 444, 2018.

13 Dumitriu, M., **Gheți, M.A.**, *Numerical study on the influence of suspension damping on the bogie vertical vibration*, IOP Conf. Series: Materials Science and Engineering, Vol. 564, 2019

14 Dumitriu, M., **Gheți, M.A.**, *On the longitudinal vibration of the railway bogie*, MATEC Web of Conferences, Vol. 290, 2019, Numărul articolului 08008.

15 Dwyer-Joyce, R. S., Yao, C., Lewis, R., Brunskill, H., *An ultrasonic sensor for monitoring wheel flange/rail gauge corner contact*, Proceedings of the Institution of Mechanical Engineers, Part F: Journal of Rail and Rapid Transit, 227(2), 188-195, 2013.

16 Dwyer-Joyce, R. S., Yao, C., Zhang, J., Lewis, R., Drinkwater, B. W., *Feasibility study for real time measurement of wheel-rail contact using an ultrasonic array*, 2009.

17 **Gheți, M.A.**, Mazilu, T., *Torsion frequency response function of a train driving wheelset*, IOP Conf. Series: Materials Science and Engineering, Vol. 997, 2020, Numărul articolului 012044.

18 Hussain, I., Mei, T. X., *Multi Kalman filtering approach for estimation of wheel-rail contact conditions*, UKACC International Conference on Control 2010 (pp. 1-6), 2010.

19 Hussain, I., Mei, T. X., Ritchings, R. T., *Estimation of wheel–rail contact conditions and adhesion using the multiple model approach*, Vehicle System Dynamics, 51(1), 32-53, 2013.

20 Iwnicki, S., Spiryagin, M., Cole, C., McSweeney, T., *Handbook of Railway Vehicle Dynamics*, Second Edition, CRC Press, Taylor& Francis Group, Boca Raton, 2020.

21 Iwnicki, S., *The Manchester Benchmarks for Rail Vehicle Simulation*, Routledge, 2017.

22 Kalker, J. J., *A Fast Algorithm for the Simplified Theory of Rolling Contact*, Vehicle System Dynamics 11, 1-13, 1982.

23 Kim, M. S., *Study on the adhesion characteristic between wheel and rail using the scaled test-bench*, Int J Mechanics, 9, 198-205, 2015.

24 Kouroussis, G., Connolly, D. P., Verlinden, O., *Railway-induced ground vibrations–a review of vehicle effects*, International Journal of Rail Transportation, 2(2), 69-110, 2014.

25 Lewis, R., Olofsson, U., *Wheel-rail interface handbook*, Elsevier, 2009.

26 Lohninger, R., Grabner, H., Weidenholzer, G., Silber, S., Amrhein, W. *Modeling, simulation, and design of a permanent-magnet-assisted synchronous reluctance machine*, IEEE Transactions on Industry Applications, 51(1), 196-203, 2014.

27 Malvezzi, M., Pugi, L., Papini, S., Rindi, A., Toni, P, *Identification of a wheel–rail adhesion coefficient from experimental data during braking tests*, Proceedings of the Institution of Mechanical Engineers, Part F: Journal of rail and rapid transit, 227(2), 128-139, 2013.

28 Martínez-Casas, J., Giner-Navarro, J., Baeza, L., Denia, F. D., *Improved railway wheelset–track interaction model in the high-frequency domain*, Journal of Computational and Applied Mathematics, 309, 642-653, 2017.

29 Mazilu, T., Dumitriu, M., *On the steady state interaction between an asymmetric wheelset and track*, Thirteenth International Conference on Civil, Structural and Environmental Engineering Computing , 2011.

30 Mazilu, T., *Analysis of infinite structure response due to moving wheel in the presence of irregularities via Green's functions method*, Proceedings of the Romanian Academy, Series A: Mathematics, Physics, Technical Sciences, Information Science, 10(2), 139-150, 2009.

31 Mazilu, T., *Confortul la materialul rulant*, Ed. Matrixrom, București, 2003.

32 Mazilu, T., **Gheți, M.A.**, Leu, M.C., *Influence of elastic supports on the dynamic response of two rails connected with joint bars*, U.P.B. Sci. Bull., Series D, Vol. 83, Iss. 3, 2021.

33 Mazilu, T., **Gheți, M.A.**, *Modelul mecanic al osiei motoare pentru studiul interacțiunii cu calea de rulare*, Simpozionul Național de Material Rulant de Cale Ferată – XVI, București, 2017, Editura MatrixRom, București, ISSN 1843-9888, ISSN 1843-9888, pp. 20-29.

34 Mazilu, T., **Gheți, M.A.**, *On the bending vibration of a train driving wheelset*, IOP Conference Series: Materials Science and Engineering, 2019, Vol. 591, Numărul articolului 012059.

35 Mazilu, T., **Gheți, M.A.**, *Regimurile staționare de tracțiune ale locomotivelor electrice*, Simpozionul Național de Material Rulant de Cale Ferată – XVII, București, 2019, Editura MatrixRom, București, ISSN 1843-9888, pp. 2-11.

36 Mazilu, T., **Gheți, M.A.**, *Theoretical assessment of vertical interaction between a wheelset and track: Influence of the track damping model*, Proceedings of the International Conference on Structural Dynamic, EURODYN 2020, Vol. 2, 2020, pp. 2667 - 2679.

37 Mazilu, T., **Gheți, M.A.**, *Vibrațiile torsionale ale osiei motoare*, Simpozionul Național de Material Rulant de Cale Ferată – Ediția XVII, București, 2018, Editura MatrixRom, ISSN 1843-9888, pp. 2-11.

38 Mazilu, T., *Green's functions for analysis of dynamic response of wheel/rail to vertical excitation*, Journal of Sound and vibration, 306(1-2), 31-58, 2007.

39 Mazilu, T., Răcănel, I.R., **Gheți, M.A.**, *Vertical interaction between a driving wheelset and track in the presence of the rolling surfaces harmonic irregularities*, Romanian Journal of Transport Infrastructure, Vol. 9, Numărul 2, 2020, pp. 38 – 52.

40 Mazilu, T., *Some aspects about Driving wheel/rail contact in steady state interaction*, 10th International Conference on Tribology, Bucharest, Romania (pp. 33-38), 2007.

41 Mazilu, T., *Vibrații roată-șină*, Ed. MatrixRom, București, 2008.

42 Mazilu, T., *Vibrații*, Ed. MatrixRom, București, 2012.

43 Mazilu, T., *Wheel/rail interaction due to parametric excitation*, Scientific Bulletin Series D: Mechanical Engineering, 69(3), 23-38, 2007.

44 Meymand, S. Z., Craft, M. J., Ahmadian, M., *On the application of roller rigs for studying rail vehicle systems*, Rail Transportation Division Conference (Vol. 56116, p. V001T01A015). American Society of Mechanical Engineers, 2013.

45 Moghaddam, R. R., Magnussen, F., Sadarangani, C. *Theoretical and experimental reevaluation of synchronous reluctance machine*, IEEE Transactions on Industrial Electronics, 57(1), 6-13, 2009.

46 Nategh, S., Lindberg, D., Brammer, R., Boglietti, A., Aglen, O., *Review and trends in traction motor design*: Electromagnetic and cooling system layouts, XIII International Conference on Electrical Machines (ICEM) (pp. 2600-2606). IEEE, 2018.

47 Onat, A., Voltr, P., *Swarm intelligence based multiple model approach for friction estimation at wheel-rail interface*, Proceedings of the 5th International Symposium on Engineering, Artificial Intelligence and Applications (ISEAIA 2017), Kyrenia, Cyprus (pp. 8-10), 2017.

48 Pau, M., Aymerich, F., Ginesu, F., *Ultrasonic measurements of nominal contact area and contact pressure in a wheel-rail system*, Proceedings of the Institution of Mechanical Engineers, Part F: Journal of Rail and Rapid Transit, 214(4), 231-243, 2000.

49 Pichlík, P., Zděnek, J., *Extended Kalman filter utilization for a railway traction vehicle slip control*, 2017 International Conference on Optimization of Electrical and Electronic Equipment (OPTIM) & 2017 Intl Aegean Conference on Electrical Machines and Power Electronics (ACEMP) (pp. 869-874). IEEE, 2017.

50 Piotrowski, J., Chollet, H., *Wheel–rail contact models for vehicle system dynamics including multi-point contact*, Vehicle System Dynamics, 43(6-7), 455-483, 2005.

51 Polach, O., *A fast wheel-rail forces calculation computer code*, Vehicle System Dynamics, 33(sup1), 728-739, 1999.

52 Polach, O., *Creep forces in simulations of traction vehicles running on adhesion limit*, Wear, 258(7-8), 992-1000, 2005.

53 Popa, G. *Tracțiune feroviară cu motoare asincrone trifazate*, Ed. Matrixrom, București, România, 2005.

54 Remington, P. J., *Wheel/rail rolling noise, I: Theoretical analysis*, The journal of the Acoustical Society of America, 81(6), 1805-1823, 1987,

55 Sebeșan, I., *Tratat de dinamica vehiculelor feroviare*, Ed. Academiei Române, București, România, 2020.

56 Sichani, M., Enblom, R., Berg, M., *An alternative to FASTSIM for tangential solution of the wheel–rail contact*, Vehicle System Dynamics, 54(6), 748-764, 2016.

57 Spiryagin, M., Cole, C., Sun, Y. Q., McClanachan, M., Spiryagin, V., McSweeney, T. *Design and simulation of rail vehicles*, CRC press, 2014.

58 Strano, S., Terzo, M., *On the real-time estimation of the wheel-rail contact force by means of a new nonlinear estimator design model*, Mechanical Systems and Signal Processing, 105, 391-403, 2018.

59 Sugiyama, H., Tanii, Y., Suda, Y., Nishina, M., Komine, H., Miyamoto, T., Chen, H., *Wheel/rail contact geometry on tight radius curved track: simulation and experimental validation*, Multibody system dynamics, 25(2), 117-130, 2011.

60 Thompson, D. J., Latorre Iglesias, E., Liu, X., Zhu, J., Hu, Z., *Recent developments in the prediction and control of aerodynamic noise from high-speed trains*, International Journal of Rail Transportation, 3(3), 119-150, 2015.

61 Thompson, D. J., *Noise and Vibration Mechanisms Modelling and Means of Control*, Elsevier, Oxford, UK, 2008.

62 Vollebregt, E. A. H., Iwnicki, S. D., Xie, G., Shackleton, P., *Assessing the accuracy of different simplified frictional rolling contact algorithms*, Vehicle System Dynamics, 50(1), 1-17, 2012.

63 Ward, C. P., Goodall, R. M., Dixon, R., Charles, G. A., *Adhesion estimation at the wheel–rail interface using advanced model-based filtering*, Vehicle System Dynamics, 50(12), 1797-1816, 2012.

64 Wu, W., Zhu, X., Quan, L., Du, Y., Xiang, Z., Zhu, X., *Design and analysis of a hybrid permanent magnet assisted synchronous reluctance motor considering magnetic saliency and PM usage*, IEEE Transactions on Applied Superconductivity, 28(3), 1-6, 2017.

65 Yu, D., Huang, X. Y., Fang, Y. T., Zhang, J., *Design and comparison of interior permanent magnet synchronous traction motors for high speed railway applications*, IEEE Workshop on Electrical Machines Design, Control and Diagnosis (WEMDCD) (pp. 58-62). IEEE, 2017.

66 Zaazaa, K. E., Schwab, A. L., *Review of Joost Kalker's wheel*-*rail contact theories and their implementation in multibody codes*, International Design Engineering Technical Conferences and Computers and Information in Engineering Conference (Vol. 49019, pp. 1889-1900), 2009.

67 Zhai, W., *Vehicle–Track Coupled Dynamics Theory and Application*, Springer, Singapore, 2019.

68 Zhai, W., Wei, K., Song, X., Shao, M., *Experimental investigation into ground vibrations induced by very high speed trains on a non-ballasted track*, Soil Dynamics and Earthquake Engineering, 72, 24-36, 2015.

69 Zhao, Y., Liang, B., *Re-adhesion control for a railway single wheelset test rig based on the behaviour of the traction motor*, Vehicle system dynamics, 51(8), 1173-1185, 2013.